AD-A052 148 COLUMBIA UNIV NEW YORK DEPT OF CIVIL ENGINEERING AN--ETC F/G 18/9
DYNAMIC ELASTIC-PLASTIC RESPONSE OF A CONTAINMENT VESSEL TO FLU--ETC(U)
FEB 78 G NIKOLAKOPOULOU, F DIMAGGIO N00014-75-C-0695

UNCLASSIFIED TR-52 NL

| OF |
AD
A052148

END
DATE
FILMED
5-78
DDC

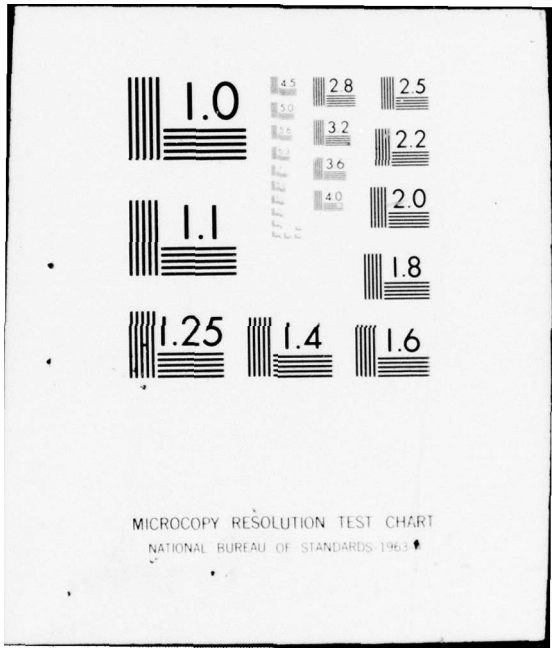
1.0
1.1
1.25
1.4
1.6
1.8
2.0
2.2
2.5
2.8
3.2
3.6
4.0
4.5
5.0
5.6
MICROCOPY RESOLUTION TEST CHART
NATIONAL BUREAU OF STANDARDS-1963-A

Columbia University
in the City of New York

DEPARTMENT OF CIVIL ENGINEERING
AND ENGINEERING MECHANICS

Dynamic Elastic-Plastic Response of a Containment Vessel To Fluid Pressure Pulses

by

G. Nikolakopoulou and F. DiMaggio

Office of Naval Research
Contract N00014-75-C-0695
Technical Report No. 52

February, 1978

DEPARTMENT OF CIVIL ENGINEERING

AND ENGINEERING MECHANICS

(6) Dynamic Elastic-Plastic Response of a Containment Vessel To Fluid Pressure Pulses,

by

(10) G. /Nikolakopoulou and F. /DiMaggio

(9) Technical rept. 31 Dec 76-30 Jun 77,

Office of Naval Research

Contract (15) NØØØ14-75-C-Ø695

Technical Report No. 52

(11) Feb[redacted]78

(14) TR-52

(12) 56 P.

"Approved for public release; distribution unlimited."

ABSTRACT

The dynamic analysis of the wall of a fluid-filled unstiffened nuclear containment vessel, to the fluid pressure exerted on it when the relief valve discharge piping is cleared, is extended into the plastic range using two versions of an elastic-plastic shell theory.

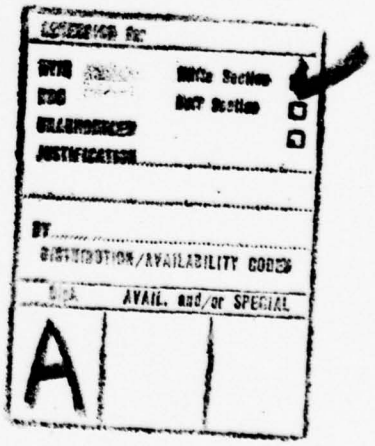

1. INTRODUCTION

In an earlier study, (Ref. [1]), a method was presented for obtaining the dynamic elastic response of a fluid-filled nuclear containment vessel when the relief valve discharge piping is cleared. In this thesis, the method is extended into the plastic range, using modified versions of a plasticity theory for shells introduced by Bieniek and Fumaro (Refs. [2], [3]). Alternatively, this investigation could have been conducted without using a shell theory. Instead, the field equations of classical elastic-plastic theory could be applied at shell layers and then integrated through the thickness (see, e.g., Refs. [4] to [8]). This latter procedure, however, may require prohibitively large computer storage capacity.

The water-filled circular cylindrical shell, shown in Fig. 1, is the model used for the lower portion of a nuclear containment vessel. It is acted upon by a cylindrical (axisymmetric) wave whose time history is shown in Fig. 2 (with magnitude normalized to 1 psi) and whose variation with depth is illustrated in Fig. 3. This approximates (see Ref. [9]) the pressure exerted on the vessel wall when the relief valve is cleared. The spatial and temporal variation of displacement, moment, and hoop stress in the cylindrical steel wall is to be determined.

2. FORMULATION OF THE PROBLEM

2.1 Fluid Equations

Assuming linear compressibility, the pressure $p(r,z,t)$ in the contained water, and its (vector) velocity $\underline{u}(r,z,t)$ satisfy the equations (Ref. [10])

$$\frac{\partial p}{\partial t} = -\rho c^2 \nabla \cdot \underline{u} \tag{1}$$

$$\rho \frac{\partial \underline{u}}{\partial t} = -\nabla p \tag{2}$$

in which: ρ is the density of water; c is the velocity of sound in water; and ∇ is the (vector) gradient operator, and the dot denotes scalar multiplication.

The continuity requirement, that the radial fluid velocity at the shell surface be equal to that of the shell, may be written as

$$\frac{\partial w}{\partial t} = u(r_1) \tag{3}$$

in which $u(r,z,t)$ is the radial component of the fluid velocity $\underline{u}$, r is the radial coordinate as in Fig. 1, and w is the radial displacement of the shell, assumed positive outward.

The boundary conditions to be satisfied are:

$$w(1,t) = 0 \tag{4}$$

$$\frac{\partial w}{\partial z}(1,t) = 0. \tag{5}$$

Equations (4) and (5) assume that the shell bottom is fixed. 1, as shown in Fig. 1 , is the depth of the shell wall.

$$\frac{\partial^2 w}{\partial z^2}(0,t) = 0 \tag{6}$$

$$\frac{\partial^3 w}{\partial z^3}(0,t) = 0 \tag{7}$$

Equations (6) and (7) assume the shell top to be free.

$$u(r_1,z,t) = 0 \qquad (0 \leq z \leq L) \tag{8}$$

Equation (8) assumes the pedestal (rigid cylindrical surface of Fig. 1) to be rigid, so that the radial fluid velocity is zero there. L is the depth of the flat rigid bottom from the free water surface, as shown in Fig. 1.

$$v(r,L,t) = 0 \qquad (r_1 \leq r \leq r_2). \tag{9}$$

Equation (9) states that the flat portion of the vessel's

bottom (see Fig. 1) is rigid, requiring that the axial component $v(r,z,t)$ of the fluid velocity $\underline{u}$ vanish there.

$$[u \sin\alpha + v \cos\alpha]_{z=l+(r_3-r)\tan\alpha} = 0 \qquad r_2 \leq r \leq r_3 \quad (10)$$

Equation (10) states that the sloping bottom of the containment vessel (see Fig. 1) is rigid, so that the component of fluid velocity normal to it is zero.

$$p(r,0,t) = 0 \quad (r_1 \leq r \leq r_3). \qquad (11)$$

Equation (11) states that the fluid pressure on the free surface is zero.

Initial rest conditions require that

$$w(r,0) = 0 \qquad (12)$$

$$\frac{\partial w}{\partial t}(z,0) = 0 \qquad (13)$$

$$p(r,z,0) = 0 \qquad (14)$$

$$\underline{u}(r,z,0) = 0 \qquad (15)$$

Note that Eqns (2), (3), (11), (12) and (14) constrain the shell displacement at the fluid surface to be zero, i.e.

$$w(0,t) = 0 \qquad (16)$$

2.2 Shell Equations

From the radial component of the shell displacement, $w(z,t)$, assumed positive outward as shown in Fig. 1, the circumferal strain ϵ and longitudinal curvature k of the shell are obtained as

$$\epsilon = \frac{w}{r_3} \tag{17}$$

$$k = \frac{\partial^2 w}{\partial z^2} \tag{18}$$

The corresponding stress resultants are, respectively, the circumferential force per unit of length, N, and longitudinal moment per unit of length, M, which satisfy the stress equation of motion (see, e.g., Ref. [11])

$$\frac{\partial^2 M}{\partial z^2} + \frac{N}{r_3} = p_I(z,t) + p(r_3,t) - \rho_s h \frac{\partial^2 w}{\partial t^2} \tag{19}$$

in which E is Young's modulus, p_I is the incident pressure of Figs. 2 and 3 caused by the relief valve clearing, ρ_s is the mass density of the shell, and h is the shell thickness.

The total strains of Eqs. (17) and (18) will be obtained as a superposition of elastic and plastic components:

$$\epsilon = \epsilon^E + \epsilon^P \tag{20}$$

$$\kappa = \kappa^E + \kappa^P \tag{21}$$

Using matrix notation,

$$\underline{e} = \begin{bmatrix} \epsilon \\ \kappa \end{bmatrix} \tag{22}$$

Eqs. (20) and (21) become

$$\underline{e} = \underline{e}^E + \underline{e}^P \tag{23}$$

2.2.1 Elastic Range

The elastic stress strain relations are (Ref. [11])

$$M = \frac{Eh^3}{12(1-\nu^2)} \kappa^E \tag{24}$$

$$N = Eh\epsilon^E \tag{25}$$

in which ν is Poisson's ratio, E is Young's modulus, and h is the shell thickness. Letting

$$\underline{s} = \begin{bmatrix} N \\ M \end{bmatrix} \tag{26}$$

and

$$\underline{E} = \begin{bmatrix} Eh & 0 \\ 0 & \dfrac{Eh^3}{12(1-\nu^2)} \end{bmatrix} \tag{27}$$

be the stress and elastic modulus matrix, respectively, Eqs. (24) and (25) may be written in matrix form as

$$\underline{s} = \underline{E}\,\underline{e}^{E} = \underline{E}\,(\underline{e} - \underline{e}^{P}) \tag{28}$$

Substituting Eqs. (17), (18), (24) and (25) into the stress equation of motion, the elastic displacement equation of motion is obtained as

$$\frac{Eh^3}{12(1-\nu^2)}\,\frac{\partial^4 w}{\partial z^4} + \frac{Eh}{r_3}\,w = p_I + p(r_3) - \rho_s h\,\frac{\partial^2 w}{\partial t^2} \tag{29}$$

2.2.2 Elasto-Plastic Range

The shell will be assumed to yield when the yield condition

$$F_0 = I_N + I_M + 2\,|I_{MN}| = 1\,, \tag{30}$$

in which

$$I_N = \left[\frac{N}{N_0}\right]^2 \tag{31}$$

$$I_M = \left[\frac{M}{M_0}\right]^2 \tag{32}$$

$$I_{MN} = \frac{MN}{2M_0N_0} \tag{33}$$

is satisfied. This relation is obtained from that general three dimensional (condition) used by Bieniek and Funaro (Ref. [2]), for the axisymmetric condition of the problem being considered, when Poisson's ratio effects (i.e., induced circumferential moments) are neglected. In Eqs. (31) - (33),

$$N_0 = \sigma_0 h \tag{34}$$

and

$$M_0 = \frac{\sigma_0 h^2}{6} \tag{35}$$

in which σ_0 is the uniaxial yield stress; N_0 and M_0 are, respectively, the axial force at which yielding occurs in the absence of bending, and bending moment at which yielding occurs in the absence of axial force, in a beam.

If circumferential moments are again ignored, the limit function suggested in Ref. [2] is

$$F_L = I_N + \frac{4}{9} I_M + \frac{2}{3\sqrt{3}} \left|I_{MN}\right| = 1 \tag{36}$$

In Fig. 4, the yield and limit surfaces corresponding to Eqs. (30) and (36) are displayed.

In conjunction with the yield and limit functions of Eqs. (30) and (36), it is proposed to use a loading function

$$F = I_N + I_M^* + \frac{2}{3\sqrt{3}} \left| I_{MN} \right| = 1 \tag{37}$$

in which

$$I_M^* = \frac{M^2 - 2MM^*}{M_0^2} \tag{38}$$

In Reference [2],

$$I_M^* = \frac{(M - M^*)^2}{M_0^2} \tag{39}$$

is used. For stress points near the axis M = 0 the resulting loading function can lead to a violation of Drucker's second postulate (Ref. [12])

$$\tilde{\underline{s}} \; \dot{\underline{e}}^P \geq 0 \; . \tag{40}^*$$

Drucker's first postulate (Ref. [12])

$$(\underline{s} - \underline{s}_0) \; \dot{\underline{e}}^P \geq 0, \tag{41}$$

* In the Appendix, an alternate procedure for overcoming this difficulty is considered.

in which s_0 is any stress point within the loading function $F=1$, is satisfied using either expression for I_M^* since the resulting loading surfaces are convex and an associated flow rule will be used.

As in Ref. [2], it is proposed that the hardening parameter M^* increase during plastic loading according to the rule

$$\frac{dM^*}{M_0} = 2(1-F_L)\,\frac{G}{G_M}\,\frac{dk^P}{k_0} \tag{42}$$

in which M_0 and k_0 are related by Eq. (24),

$$G = \left\{\left[\frac{\partial F}{\partial(N/N_0)}\right]^2 + \left[\frac{\partial F}{\partial(M/M_0)}\right]^2\right\}^{1/2} \tag{43}$$

is the absolute value of the gradient of the loading surface in nondimensional space, and

$$G_M = \left|\frac{\partial F}{\partial(M/M_0)}\right| \tag{44}$$

is that part of G contributed by bending.

The resulting loading function, shown in Fig. 4, exhibits features of both kinematic and isotropic hardening. Whenever $F=1$ lies outside $F_L=1$, $F_L=1$ is used to determine $\underline{\epsilon}^P$.

Plastic loading is defined to occur when Eq. (37) is satisfied and

$$\delta F = \frac{\partial F}{\partial N} \dot{N} + \frac{\partial F}{\partial M} \dot{M} > 0 \tag{45}$$

in which dots denote differentiation with respect to time. (Unloading, which is elastic, is characterized by $\delta F < 0$, while for neutral loading, during which the stress point moves on the loading surface but no hardening occurs, $\delta F = 0$). Letting

$$\frac{\partial F}{\partial \underline{s}} = \begin{bmatrix} \frac{\partial F}{\partial N} \\ \\ \frac{\partial F}{\partial M} \end{bmatrix} \tag{46}$$

The loading condition of Eq. (45) may be written as

$$\delta F = \frac{\widetilde{\partial F}}{\partial \underline{s}} \dot{\underline{s}} > 0 \tag{47}$$

in which the symbol $\sim$ denotes transpose.

The plastic strain increment is obtained from the loading function by an associated flow rule

$$\dot{\underline{e}}^P = \lambda \frac{\partial F}{\partial \underline{s}} \tag{48}$$

in which

$$\lambda = \frac{\frac{\tilde{\partial}F}{\partial \underline{s}} \underline{E} \dot{\underline{e}}}{\frac{\tilde{\partial}F}{\partial \underline{s}} \underline{E} \frac{\partial F}{\partial \underline{s}} - \frac{\partial F}{\partial \underline{s}^*} A \frac{\partial F}{\partial \underline{s}}} \tag{49}$$

with

$$\underline{s}^* = \begin{bmatrix} 0 \\ M^* \end{bmatrix} \tag{50}$$

and

$$A = 2(1-F_L) \frac{M_0}{k_0} \frac{G^2}{G_M^2} \tag{51}$$

Eq. (49) is obtained by differentiating Eq. (37) and using Eqs. (28), (42) and (48).

Substituting Eq. (49) into Eq. (28) differentiated with respect to time yields

$$\dot{\underline{s}} = \underline{D} \dot{\underline{e}} \tag{52}$$

in which

$$\underline{D} = \underline{E} \left[\underline{1} - \frac{\frac{\tilde{\partial}F}{\partial \underline{s}} \underline{E} \frac{\partial F}{\partial \underline{s}}}{\frac{\tilde{\partial}F}{\partial \underline{s}} \underline{E} \frac{\partial F}{\partial \underline{s}} - \frac{\tilde{\partial}F}{\partial \underline{s}^*} A \frac{\partial F}{\partial \underline{s}}} \right] \tag{53}$$

is the elastic-plastic tangent stiffness.

It should be noted that, substituting Eq. (52) into Eq. (40), Drucker's second postulate becomes equivalent to the requirement that $\underline{D}$ be positive definite.

3. METHOD OF SOLUTION

The finite element method utilized for the fluid equation and the elastic phase of the shell motion are identical to those described in Ref. [1] and will not be repeated here. The two-dimensional grid and molecule used for the fluid equation, like the one displayed in Fig. 5, and the one dimensional grid used for the elastic phase of the shell motion, shown in Fig. 6, are also used for the plastic phase.

In what follows the iterative computational scheme utilized in the (nonlinear) plastic phase is outlined. In all cases where equations are referenced, the finite difference form of the equation was used.

Assume that at a time t_i, when the incident pressure $p_I(t_i)$ is acting, the stress $\underline{s}(t_i)$ strain $\underline{e}(t_i)$ and displacement $w(t_i)$ in the shell, and the velocity $\underline{u}(t_i)$ and induced pressure $p(t_i)$ corresponding to a grid point are known. In this notation and that which follows in this section, the spatial dependence, usually expressed with subscripts in finite difference form, is supressed. Let $M^*(t_i)$ denote the value of the hardening parameter at t_i which is the same as the value at the end of the last plastic phase preceding time t_i and let $F(t_i)$ denote the loading function of Eq. (37). Then

$$F(t_i) \begin{matrix} < 1 \\ = 1 \end{matrix} \text{ if } t_i \text{ corresponds to an } \begin{matrix} \text{elastic} \\ \text{plastic} \end{matrix} \text{ state} \quad (54)$$

At a time $t_i+\Delta t$, when the incident pressure is $p_i(t_i+\Delta t)$, $w(t_i+\Delta t)$ is obtained from Eq. (19) and then $\underline{e}(t_i+\Delta t)$ from Eqs. (17) and (18). The elastic stress increment corresponding to the strain increment

$$\Delta\underline{e} = \underline{e}(t_i + \Delta t) - \underline{e}(t_i) \tag{55}$$

is obtained from

$$(\Delta\underline{s})_1 = E\ \Delta\underline{e} \tag{56}$$

in which the subscript 1 denotes a first approximation to the value which would be obtained from Eq. (28) if $\underline{e}^P$ were known. Correspondinly, a stress

$$\underline{s}_1(t_i + \Delta t) = \underline{s}(t) + (\Delta\underline{s})_1 \tag{57}$$

can be calculated and substituted into the loading function

$$F_1(t_i + \Delta t) \quad \begin{cases} < 1 & \text{(58a)} \\ = 1 & \text{(58b)} \\ > 1 & \text{(58c)} \end{cases}$$

Case a can occur only if an elastic change occurs. Thus

$$\underline{s}_1(t_i + \Delta t) = \underline{s}(t + \Delta t) \tag{59}$$

and the value of all other response functions at $t=t_i+\Delta t$ are readily determined.

Case b occurs if an elastic loading brings the stress point to, or keeps it on, the loading surface and Eq. (59) again holds. For both cases a and b, no updating of the hardening parameter M^* occurs.

Case c indicates that plastic strain has occured and that $(\Delta s)_1$ computed from (56) is an upper bound to the correct Δs. As a first correction, determine λ_1 using Eq. (49) with F_1, s_1 and the last update of M^*. This requires utilization of Eqs. (43), (44) and (51). Now $(\Delta \underline{e}^P)_1$ is obtained from Eq. (48) and a second approximation to $\underline{s}(t_i + \Delta t)$ is obtained from Eq. (28) as

$$\underline{s}_2(t_i + \Delta t) = \underline{E}\left[\underline{e} - (\underline{e}^P)_1\right] \tag{60}$$

Using $\underline{s}_2$, a new value $F_2(t_i + \Delta t)$ is obtained from Eq. (37). If F_2 is ~ 1,

$$F_2(t_i + \Delta t) = F(t_i + \Delta t) \tag{61}$$

and

$$\underline{s}_2(t_i + \Delta t) = \underline{s}(t_i + \Delta t) \tag{62}$$

If F_2 is still > 1 by too much, a second iteration is necessary.

When Eq. (61) is held to be valid, a check is made to see that plastic loading has occured, using Eq. (45). if Eq. (45) is satisfied M^* is updated using Eq. (42).

The procedure outlined above is illustrated in Fig. 7.

As can be seen in Fig. 4, there are corners in the loading function along the M and N axes. At these corners where two loading surfaces F_a and F_b meet, as in Fig. 8, the strain increment is obtained from the linear combination (Ref. [13])

$$\dot{\underline{e}}^P = \lambda_a \frac{\partial F_a}{\partial \underline{s}} + \lambda_b \frac{\partial F_b}{\partial \underline{s}} \tag{63}$$

which replaces Eq. (48). In Eq. (63), λ_a and λ_b are obtained from Eq. (49) with $F = F_a$ and F_b , respectively.

CHAPTER 4

NUMERICAL RESULTS

A steel shell and water, with the following geometrical and material parameters were used:

h	= 1.44 in.	(.0366 m)
l	= 20 ft - 2 in.	(6.143 m)
d	= 5 ft - 6 in.	(1.676 m)
r_3	= 42 ft - 10.5 in.	(13.07 m)
r_2	= 24 ft - 0 in.	(7.315 m)
r_1	= 15 ft - 2 in.	(4.623 m)
L	= 30 ft - 11 in.	(9.423 m)
ρ	= 1.94 lb sec^2/ft^4	(2.073 x 10^7 kg/m^3)
ρ_s	= 14.9 lb sec^2/ft^4	(15.92 x 10^7 kg/m^3)
E	= 30 x 10^6 lb/in^2	(2.068 x 10^{11} N/m^2)
c	= 4790 ft/sec	(1460. m/s)
σ_o	= 3600 lb/in^2	(2.48 x 10^8 N/m^2)

The above values are the same as for the problem treated in Ref. [1] , except that the shell considered here is unstiffened.

Before proceding to the numerical solution of this problem, the elastic portion of the program to be used, modified to account for the stiffeners, was used to solve the problem of Ref. [1] . A very close numerical check was obtained.

The following numerical results were then obtained for the elastic-plastic problem, using a maximum incident pressure of

$$(p_I)_{max} = 50 \text{ psi} \quad (3.45 \times 10^5 \text{ N/m}^2)$$

and a time step

$$t = .0002 \text{ sec} \ ;$$

In Fig. 9, the history of the moment at the base of the shell, where yielding first occurs, is shown and compared with what would have been obtained elastically. It is seen that yielding first occurs at $t \sim .12$ sec, i.e. during the second spike of the incident pressure of Fig. 3 (scaled up to a maximum of 50 psi) and that the limit moment is reached at $t = .22$ sec, i.e., during the third spike in p_I and at $t = .36$ sec during the fifth spike . It should be noted that this graph and those that follow were plotted using values for each 40 time steps, i.e., for increments of .008 seconds.

In Fig. 10, the moment diagram when the limit moment is reached at the base is displayed, showing clearly that the plastic zone due to bending is confined to the immediate vicinity of the base.

In Fig. 11, a plot of the value of the loading function at the instant when the limit moment is first reached is

shown. Note that two internal plastic regions are primarily to hoop stresses.

Fig. 12 compares the history of shell displacement near the shell center (grid point $\alpha = 8$) with what would have been obtained in a purely elastic response. After initial yielding at $t=.128$ sec the plastic displacement approaches a damped oscillation about a permanently deformed configuration. The displacement diagram which looks like Fig. 13 at first yielding, displays this permanent set in the displacement at grid point $\alpha = 8$ in Figs. 14a and 14b, when its value reaches a maximum and a minimum, respectively, but does not pass through zero.

Fig. 15 is a plot of the hoop force at grid point $\alpha = 8$ as a function of time. The limiting value of $N=N_0$, is reached twice, at $t = .24$ sec, ant at $t = .232$ sec. At the later time the distributions of hoop stress and plastic zones are shown in Figs. 16 and 17.

Fig. 18 illustrates the hoop stress-strain diagram for grid point $\alpha = 8$. Within the global loading path denoted by (5) , some local unloading occurs. The corresponding moment-curvature path for the base of the shell is shown in Fig. 19.

Using the finite difference form of the equation

$$V = \frac{\partial M}{\partial x} \qquad (64)$$

the shear can be obtained. Its time history at the base and distribution when the limiting moment is reached there are displayed in Figs. 20 and 21, respectively.

Fig. 22 shows the induced fluid pressure on the shell wall at grid point $\alpha = 8$ superimposed on the incident pressure there. The total pressure on the wall is obtained by superposition of these curves.

ACKNOWLEDGEMENT

The authors are grateful to Professor Maciej Bieniek for his frequent consultation and many helpful suggestions.

APPENDIX I

In order to avoid the possibility of violating Drucker's second postulate, Eq. (40), it is not necessary to change I_M^* from the expression, Eq. (39), proposed in Ref. [2], to one like Eq. (36). Indeed, in a problem involving a general state of stress in the shell, it may not be easy to find a substitute expression. Instead, Eq. (39) can be used and the positive definiteness of $\underline{D}$ (or the positiveness of λ) checked by monitoring that

$$\beta = \frac{\tilde{\partial} F}{\partial \underline{s}^*} A \frac{\partial F}{\partial \underline{s}} \leq 0 \qquad \text{(A1)}$$

If $\beta > 0$, set $\beta = 0$ in Eqs. (49) and (53) and treat the shell as ideally plastic for that time increment. This preserves the physically desirable softening in N for stress points close to the N axis.

The calculations described in Section 4 were repeated using the modified procedure discussed in this Appendix. Comparison of peak values using the two proposed methods are made in Table I. It is readily seen that both methods produce essentially the same results.

CONCLUSION

A finite difference technique has been developed for obtaining the axisymmetric dynamic elastic-plastic response of a fluid-filled, unstiffened shell using shell theory (as opposed to three dimensional equations and integrating through the thickness) in both elastic and plastic ranges. The method is then used, in two variations, to obtain the response of the wall of a water filled, nuclear containment vessel when the relief valve discharge piping is cleared and fluid pressures exerted on it large enough to exceed the elastic range.

TABLE I

COMPARISON OF RESULTS OBTAINED USING MODIFIED METHOD OF APPENDIX AND ORIGINAL METHOD PROPOSED IN SECT. 2.2.2

	ORIGINAL		MODIFIED		% DIFF.
DISPLACEMENTS (PEAK)	Inches	Meters	Inches	Meters	
	2.76	.07	2.75	.069	.40
	1.9	.0482	1.89	.048	1.26
	3.8	.0965	3.79	.0962	.20
	3.08	.0782	3.02	.0767	1.17
MOMENTS (PEAK)	Lb. inch	Joules	Lb. inch	Joules	
	15493.8	1750.47	15503.7	1751.59	.06
	-18056.0	-2039.95	-17937.4	-2026.55	.77
	10936.3	1235.59	10895.4	1230.95	.40
	- 9363.2	-1057.84	- 9359.6	-1057.44	.04
	18195.5	2055.71	18010.0	2034.75	1.00
	-17094.7	-1931.34	-16994.0	-1919.97	.60
	13028.4	1471.94	12983.2	1466.83	.40
CIMCUMFERENTIAL FORCES (PEAK)	Lbs/inch	N/m	Lbs/inch	N/m	
	51790.9	9.1×10^6	51768.3	9.1×10^6	.04
	-51743.7	-9.1×10^6	-51762.7	-9.1×10^6	.04
	37041.9	6.5×10^6	36820.2	6.4×10^6	.60
	-45762.0	-8.0×10^6	-45688.8	-8.0×10^6	.20
	51281.1	8.9×10^6	51192.1	8.9×10^6	.17
	-51747.7	-9.1×10^6	-51432.5	-9.0×10^6	.60

Appendix II - References

1. F.L. DiMaggio, J.M. McCormick and H.H. Bleich, "Dynamic Response of a Containment Vessel to Fluid Pressure Pulses", Computers and Structures, Paper 478 (1977), pp. 1-9.
2. M.P. Bieniek and J.R. Funaro, "Elasto-Plastic Behavior of Plates and Shells", Technical Report DNA 3954 T, Defense Nuclear Agency, Weidlinger Associates, New York, N.Y., 31 March 1976.
3. M.P. Bieniek and J.R. Funaro, "Modeling of Elasto-Plastic Shells", Proc. 2nd Annual Engr. Mechanics Division Specialty Conf., North Carolina State Univ., Rayleigh, N.C., May 23-25, 1977, pp. 97-100.
4. P.V. Marcal and J.F.McNamara, "Incremental Stiffness Method for Finite Element Analysis of Nonlinear Dynamic Problems", International Symposium on Numerical and Computer Methods in Structural Mechanics, Urbana, Ill., September 1971.
5. W.E. Haisler, and D.K. Vaughan, "DYNAPLAS II- A Finite Element Program for Dynamic Large Deflection, Elasto-Plastic Analysis of Stiffened Shells of Revolution", TEES-2926-73-2 and SLA-73-1106, Texas A & M University, College Station, Texas, October 1973.
6. D. Bushnell, "A Strategy for the Solution of Problems Involving Both Large Deflections and Nonlinear Material Behavior", Symposium on Approximations and Numerical Methods for the Study of Inelastic Shells, Georgia Inst. of Technology, Atlantic, Georgia, May 1975.

7. C.M. Ni and L.H.N. Lee, "Dynamic Behavior of Cylindrical Shells at Finite Deformation", Int. J. of Non-Linear Mechanics, Vol. 9 (1974) pp.193-207.

8. R.W.H Wu and S.A. Witmer, Analytical and Experimental Studies of Nonlinear Trans. Responses of Stiffened Cylindrical Panels, AIAA Journal, V. 13, N. 9 (Sept 1975) pp 1171-1178.

9. Mark II Containment Vessel Dynamic Forcing Function Information Report. Prepared by General Electric Company, Sargent and Lundy, NEDO-21061 (Sept. 1975).

10. H. Lamb, Hydrodynamics, Dover Publications, New York, N.Y. (1932).

11. S. Timoshenko and S. Woinowsky-Krieger, Theory of Plates and Shells, Second Ed., Mc Graw-Hill, 1959.

12. D. Drucker, "On Uniqueness in the Theory of Plasticity", Q. App. Math., Vol. 14 (1956),pp 35-42.

13. W. Koiter, "Stress-Strain Relations, Uniqueness and Variational Theorems for Elastic-Plastic Materials with a Singular Yield Surface", Q. Appl. Math., Vol. 11 (1953),pp 350-354.

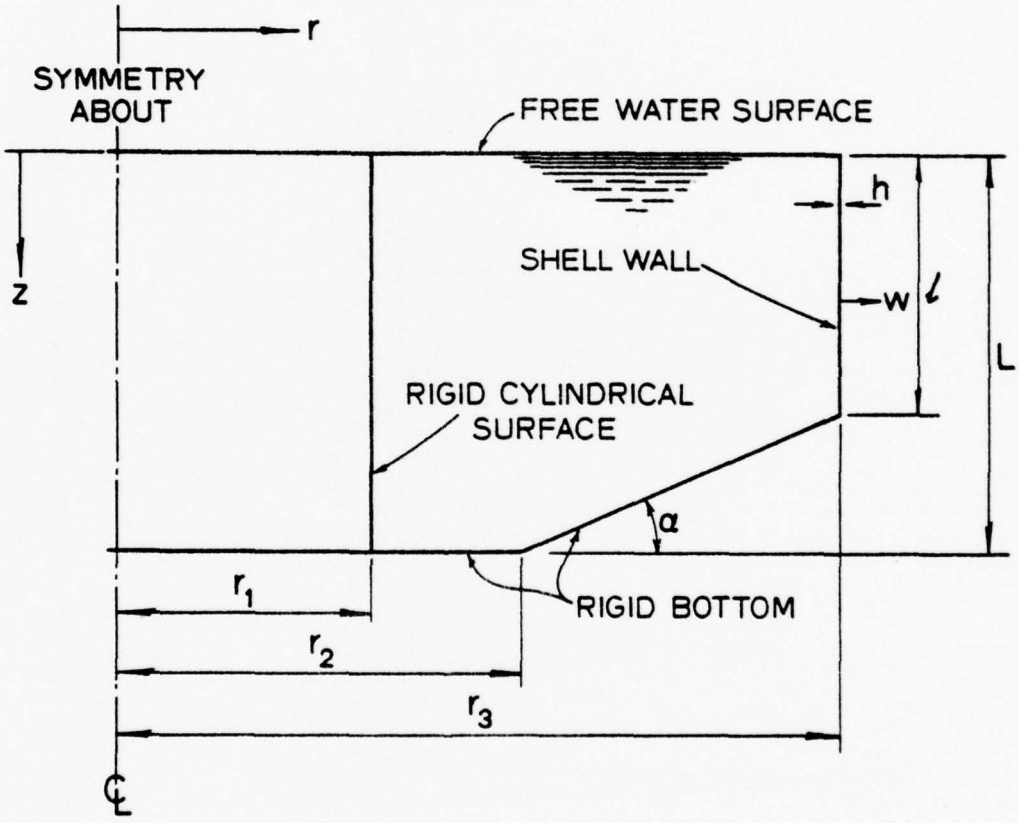

Fig. 1. Model of containment vessel analyzed

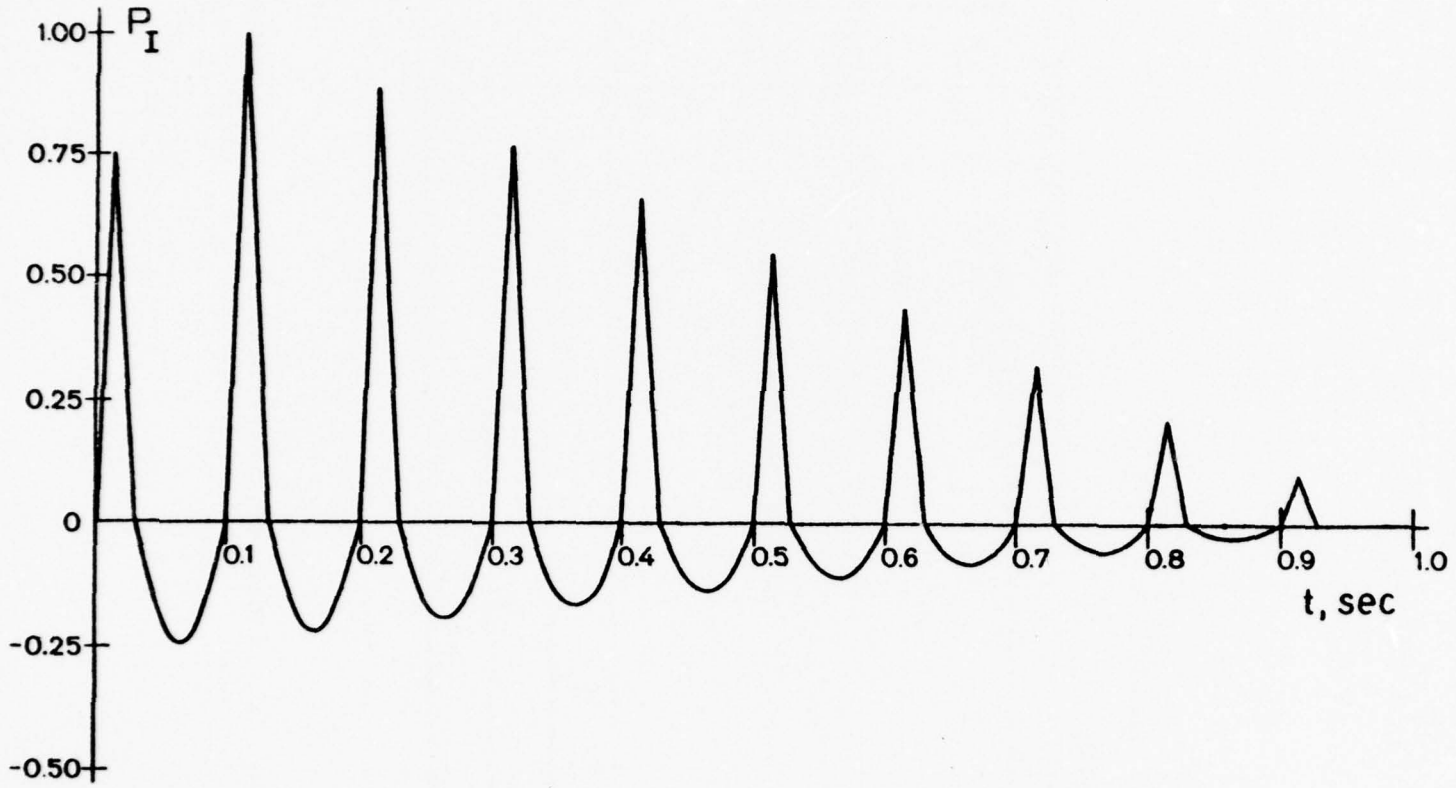

Fig. 2. Time history of incident pressure $P_I(z,t)$ (normalized to 1 psi)

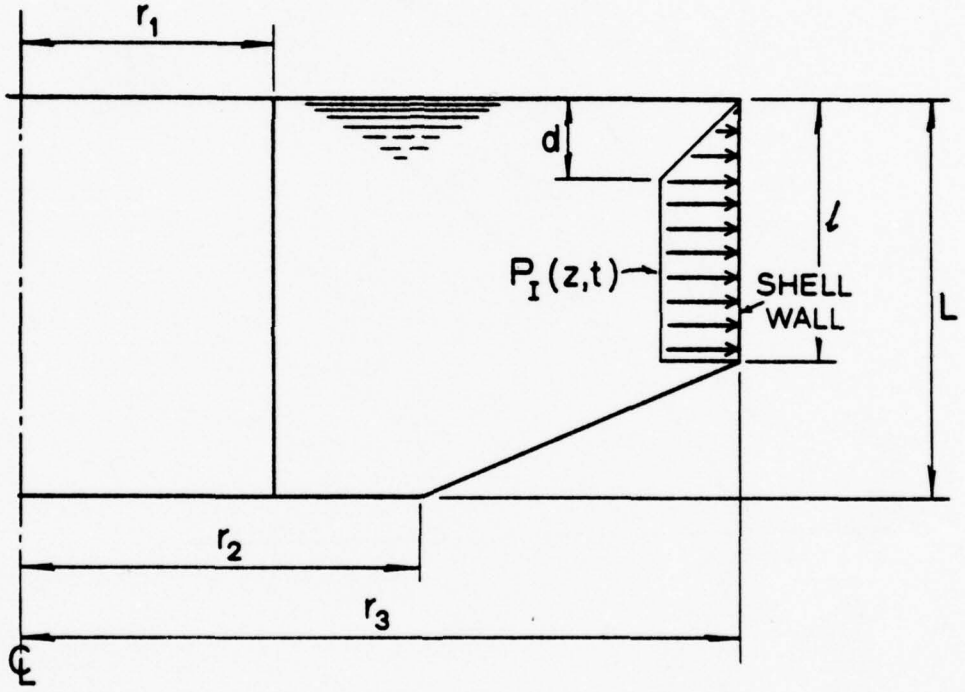

Fig. 3. Variation of incident pressure $P_I(z,t)$ with depth

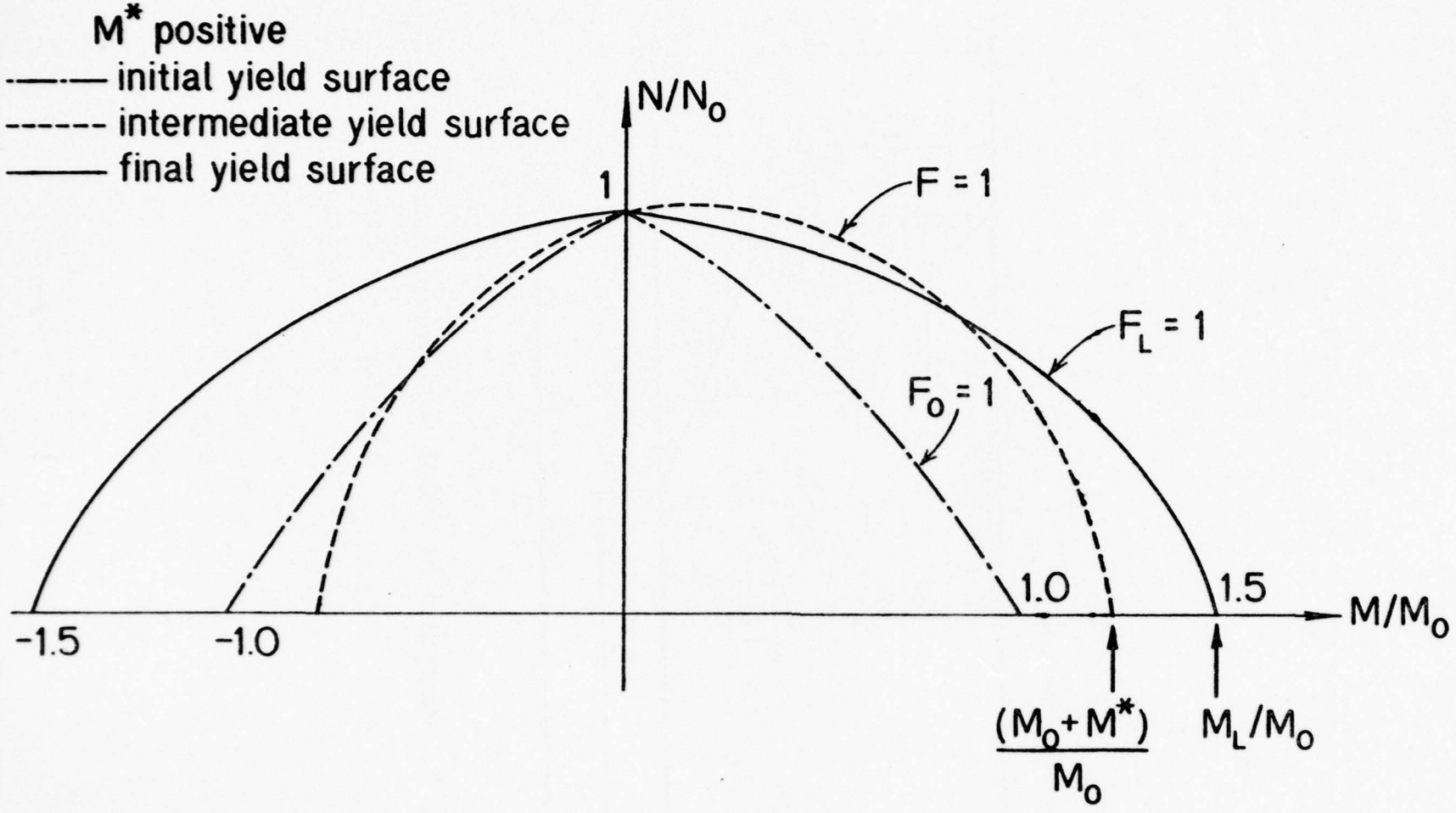

Fig. 4. Yield, limit and loading surfaces

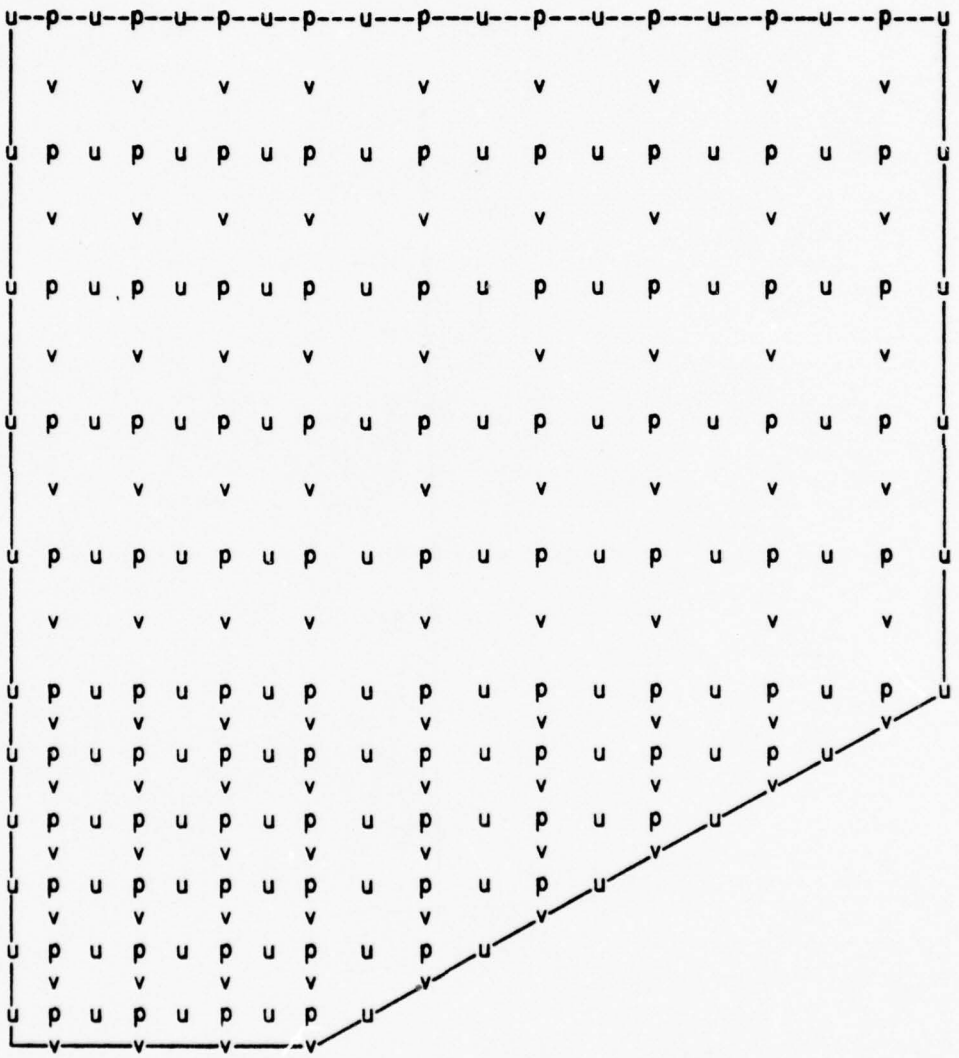

Fig. 5. Course distribution of finite difference molecules used for fluid

Fig. 6. Grid on shell surface

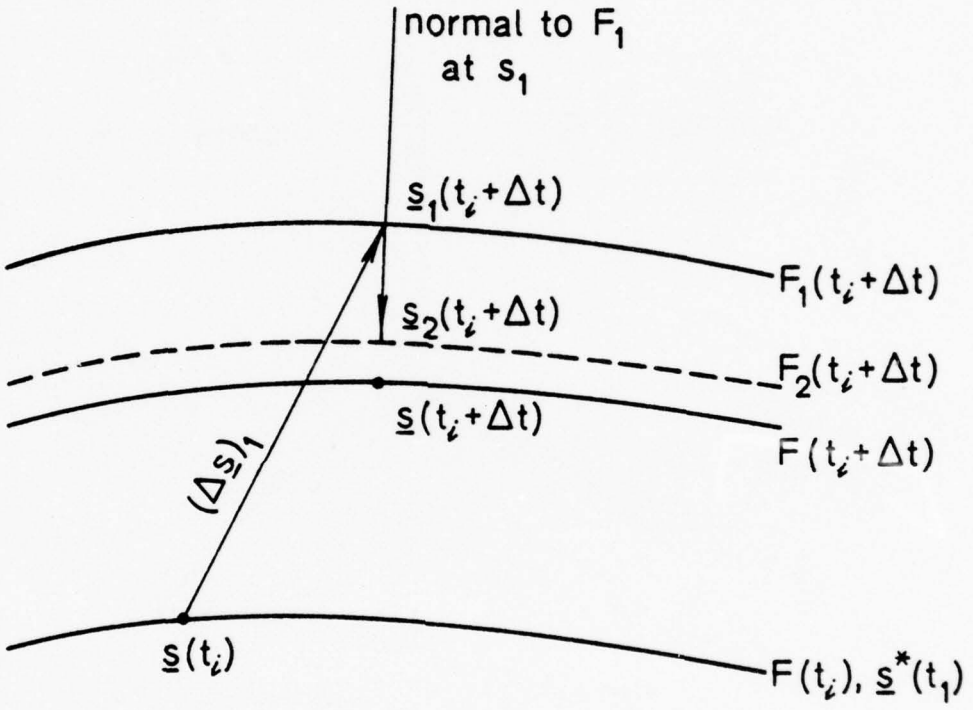

Fig. 7. Iterative scheme for plastic loading

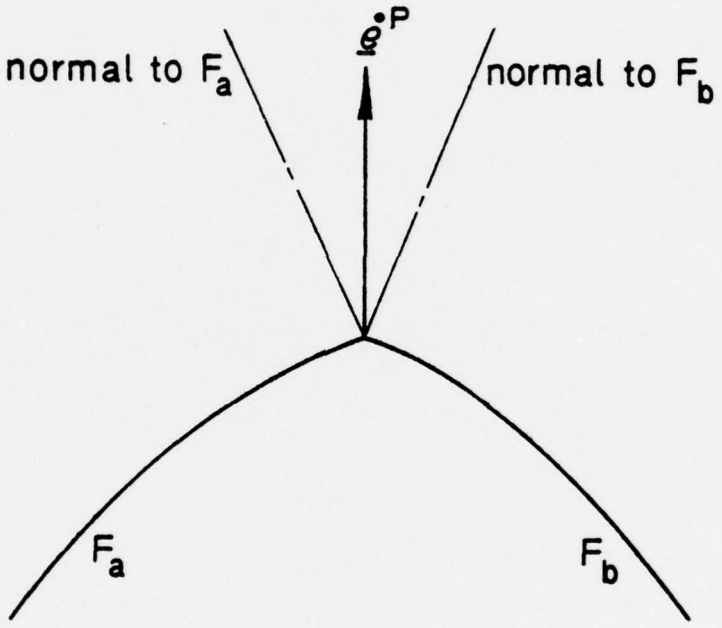

Fig. 8. Strain increment at a corner

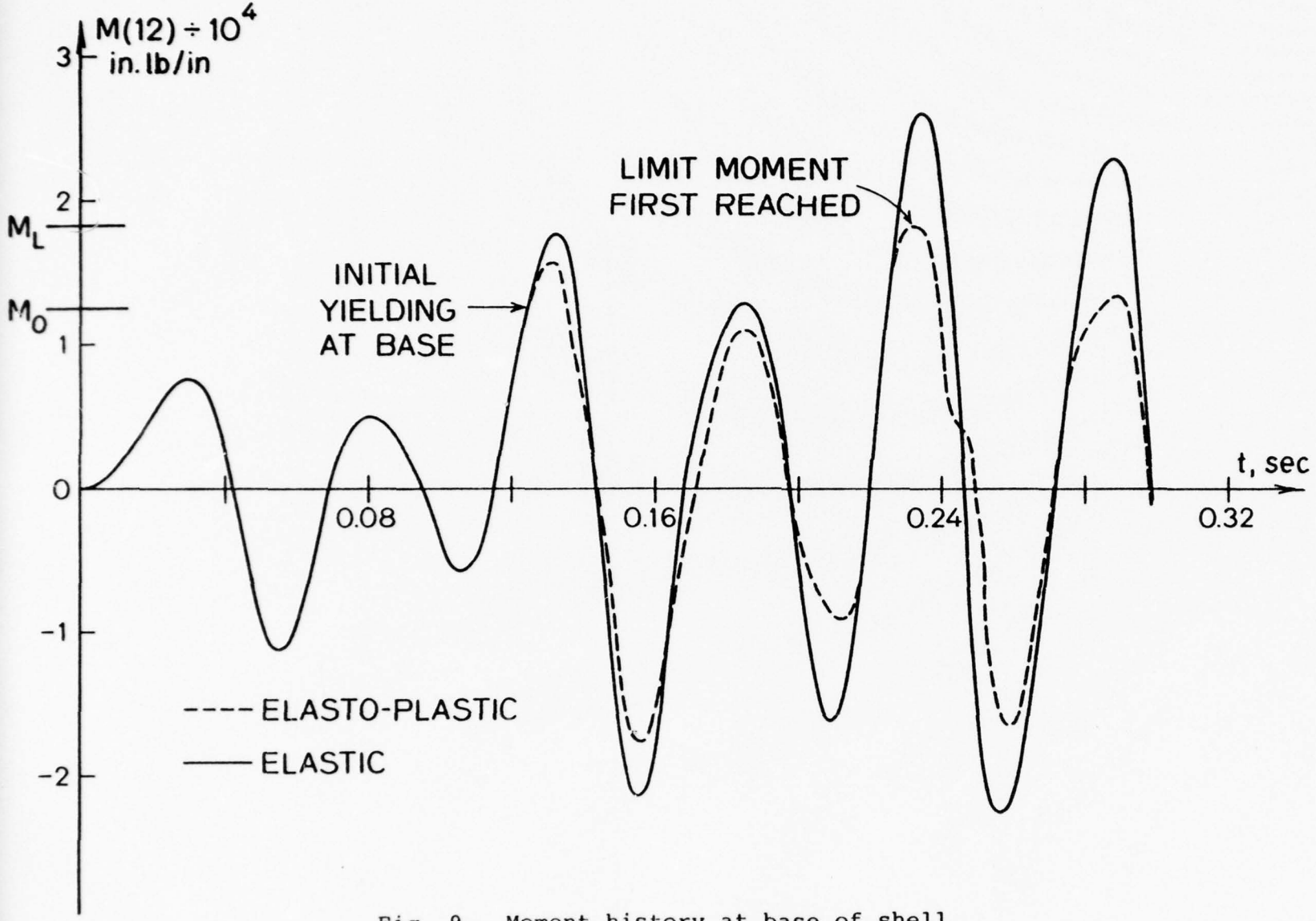

Fig. 9. Moment history at base of shell

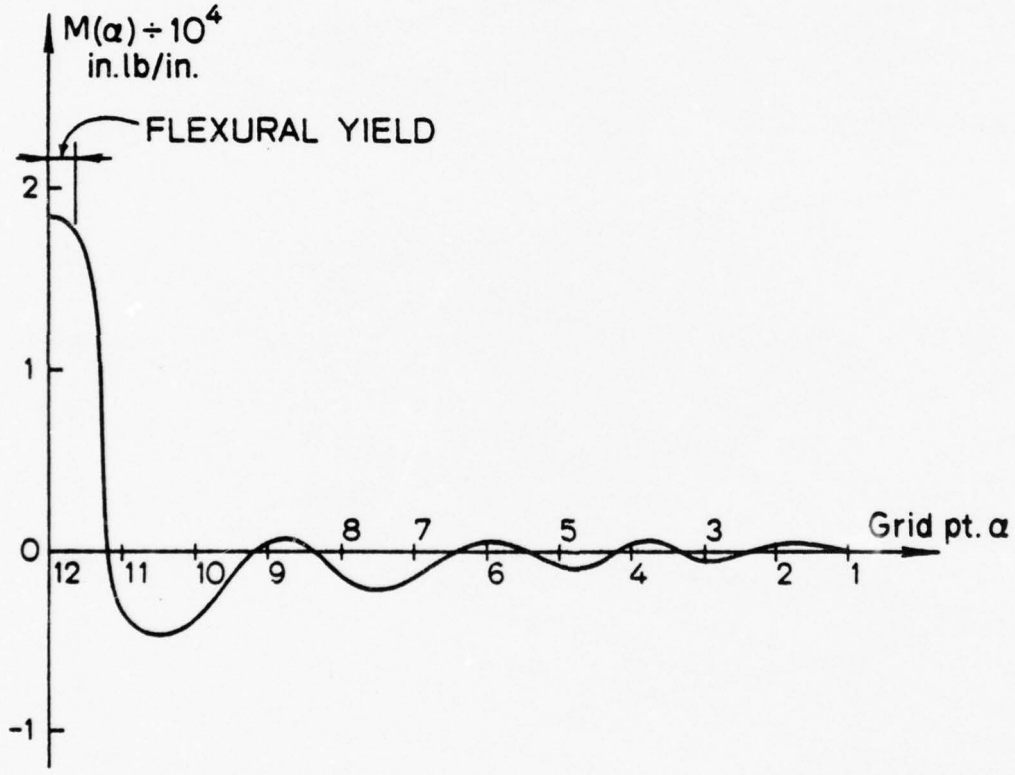

Fig. 10. Bending moment diagram when limit moment first reached

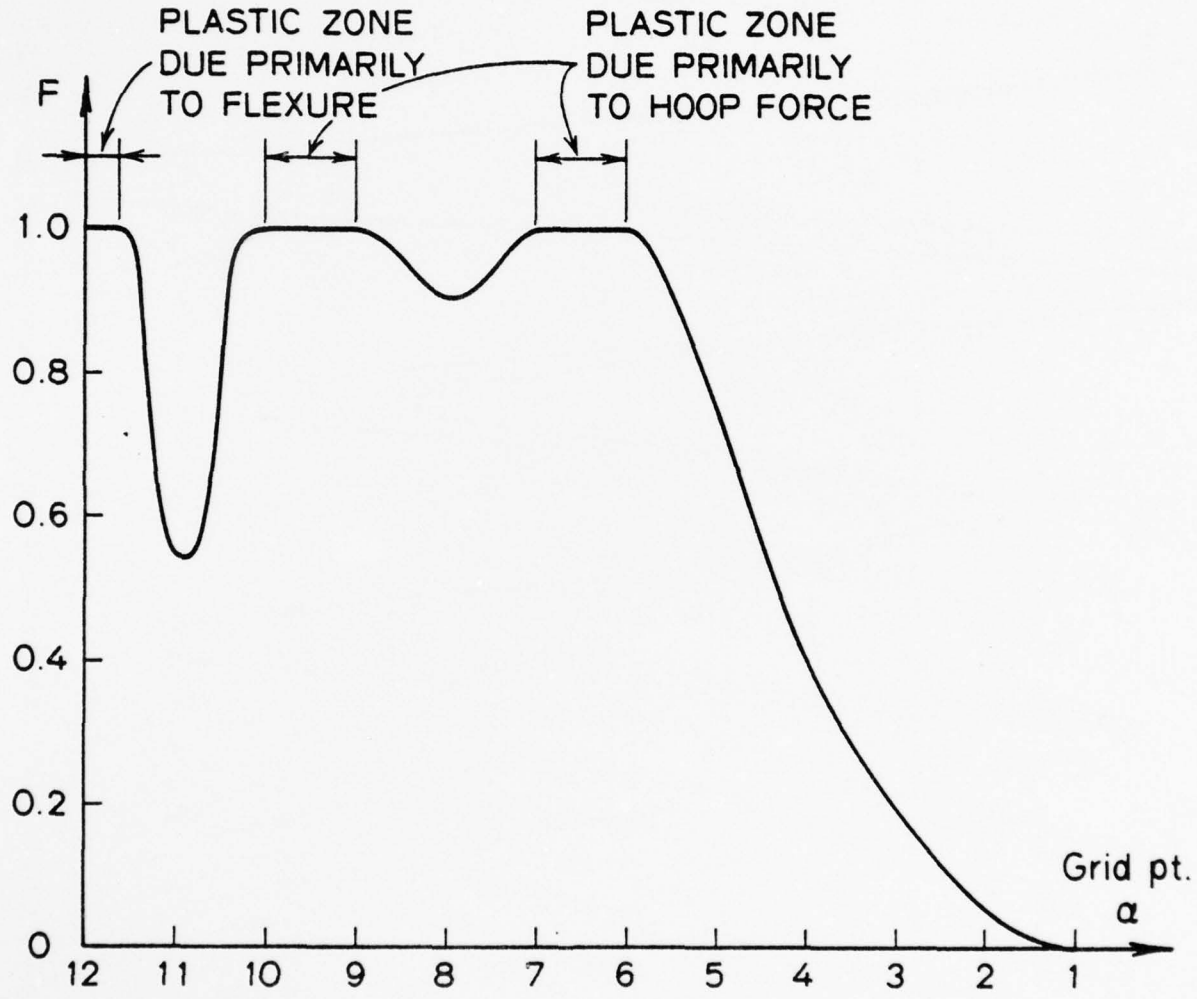

Fig. 11. Yield diagram when limit moment first reached

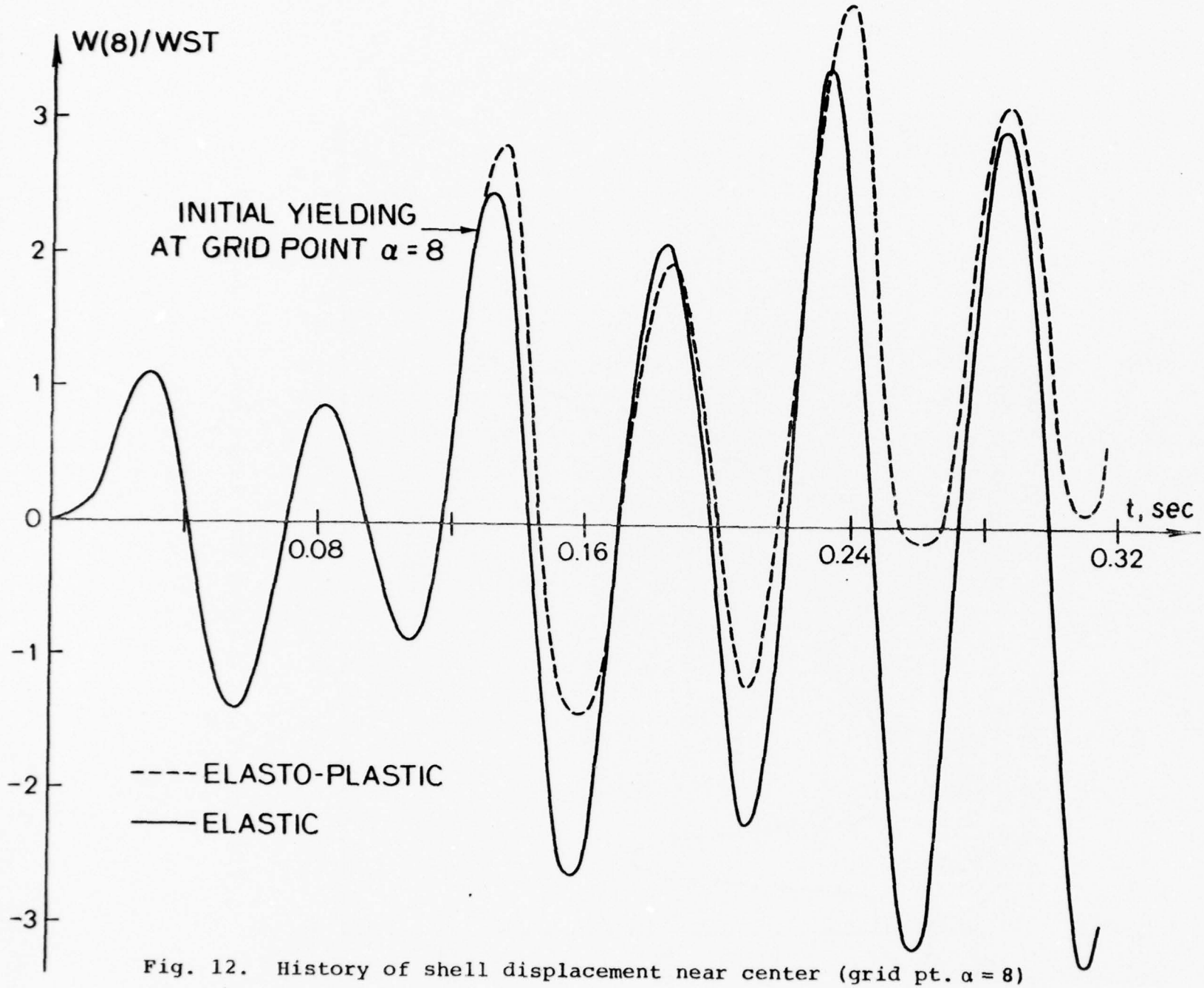

Fig. 12. History of shell displacement near center (grid pt. α = 8)

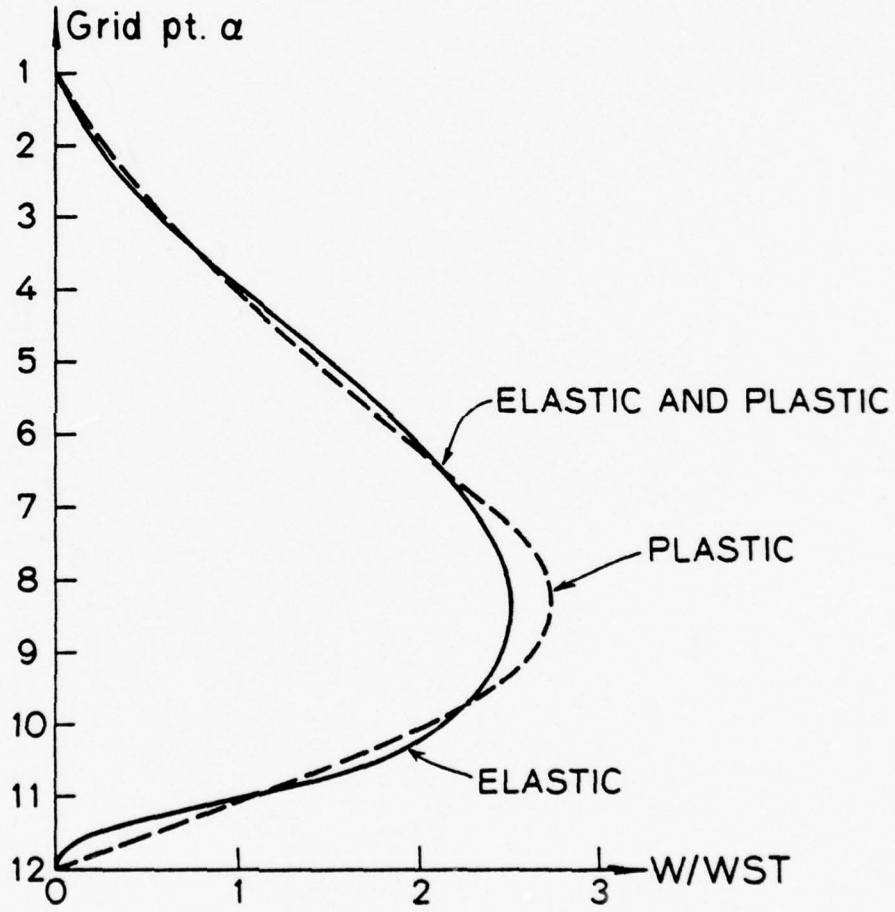

Fig. 13. Displacement of shell just after initial yielding of base (t = .132 sec)

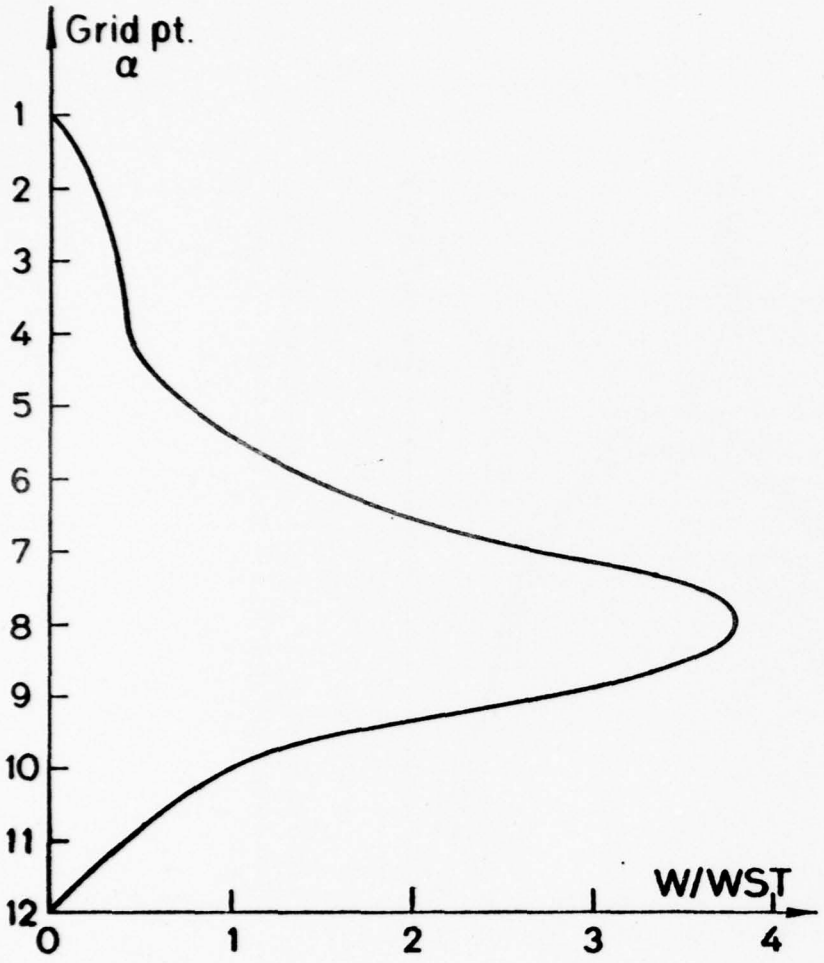

Fig. 14a. Shell displacement at t = .24 sec

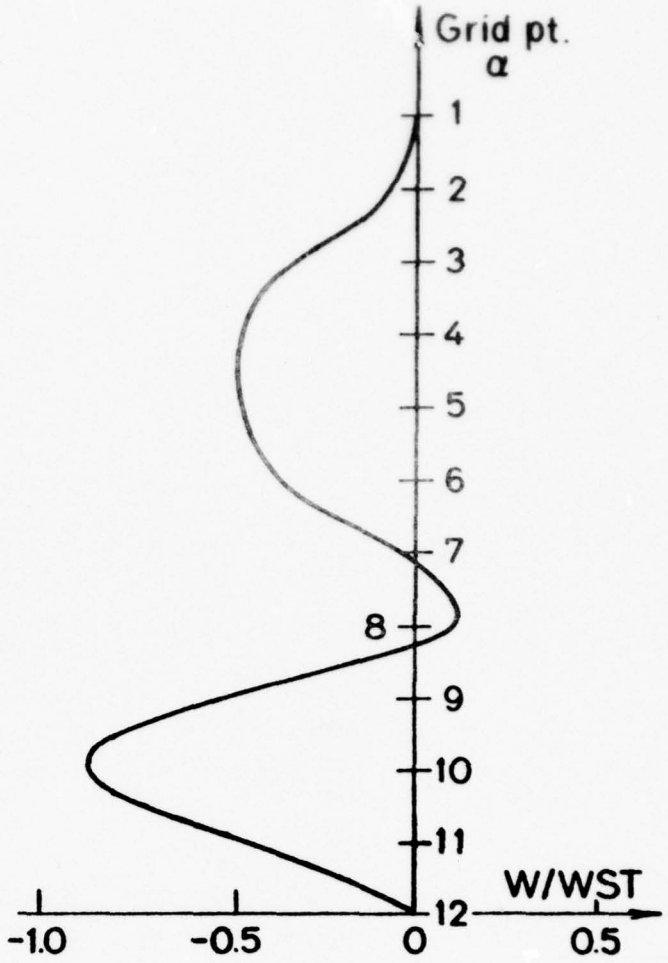

Fig. 14b. Shell displacement at t = .31 sec

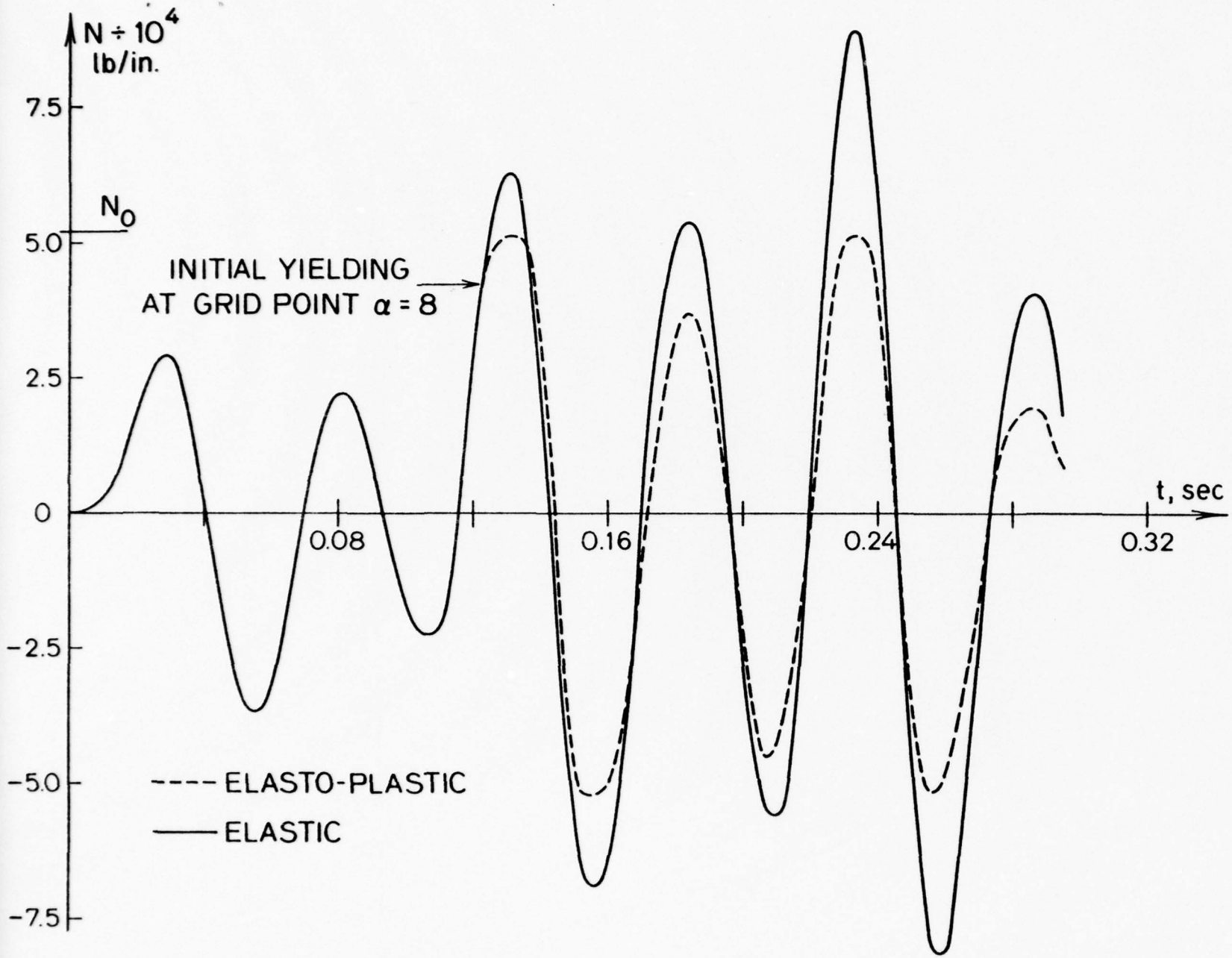

Fig. 15. Hoop force near center of shell (at grid pt. $\alpha = 8$)

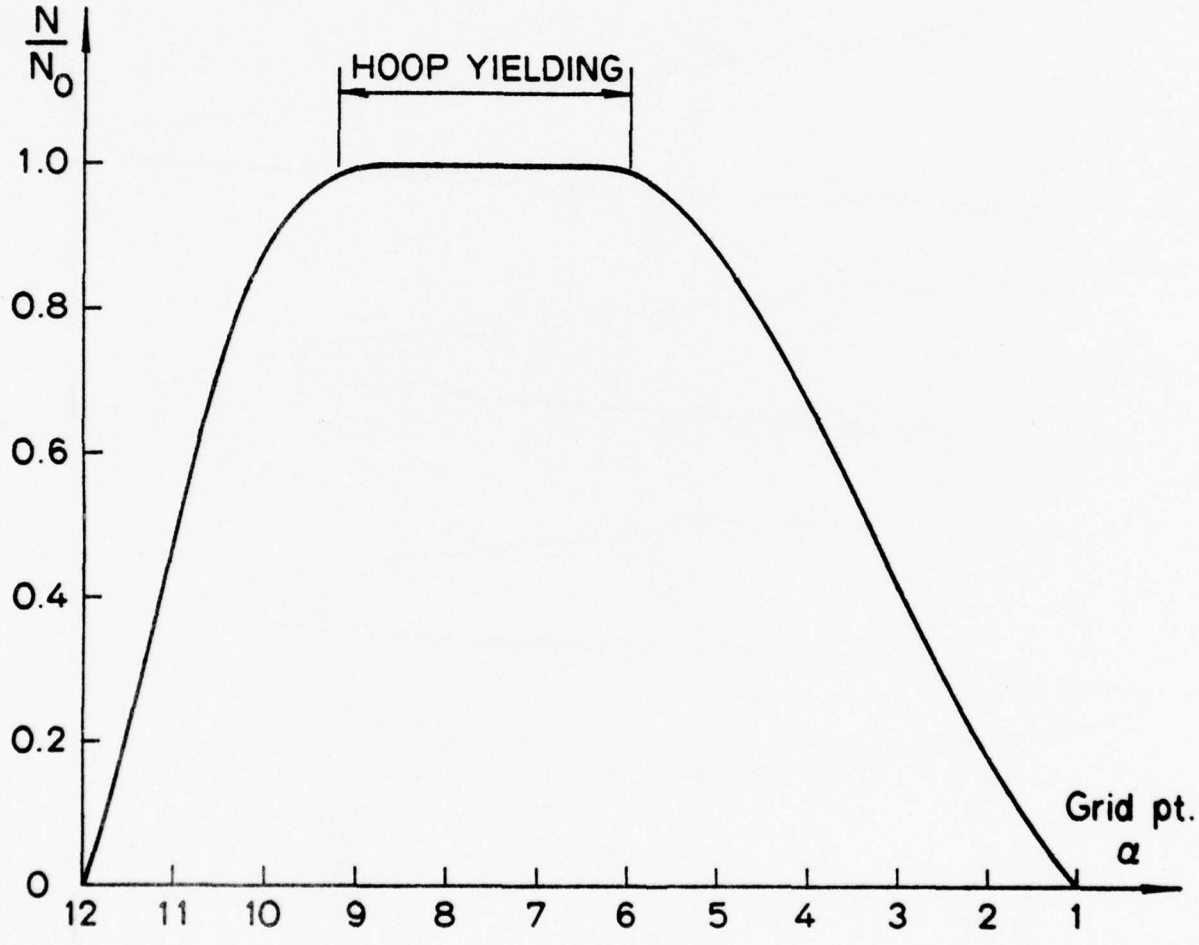

Fig. 16. Hoop stress diagram at t = .232 (when $N \sim N_o$ at $\alpha = 8$)

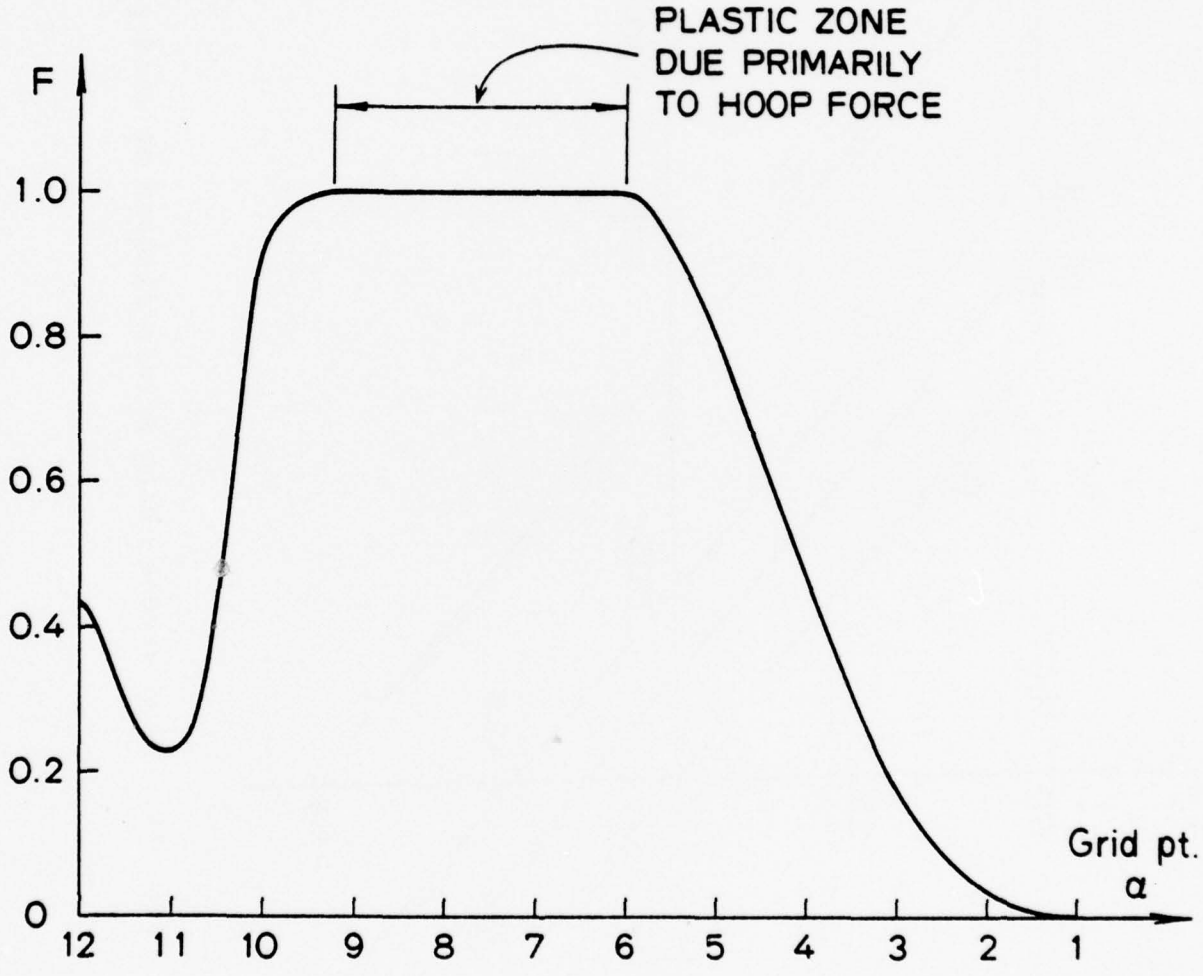

Fig. 17. Yield diagram at $t = .232$ (when $N = N_o$ at $\alpha = 8$)

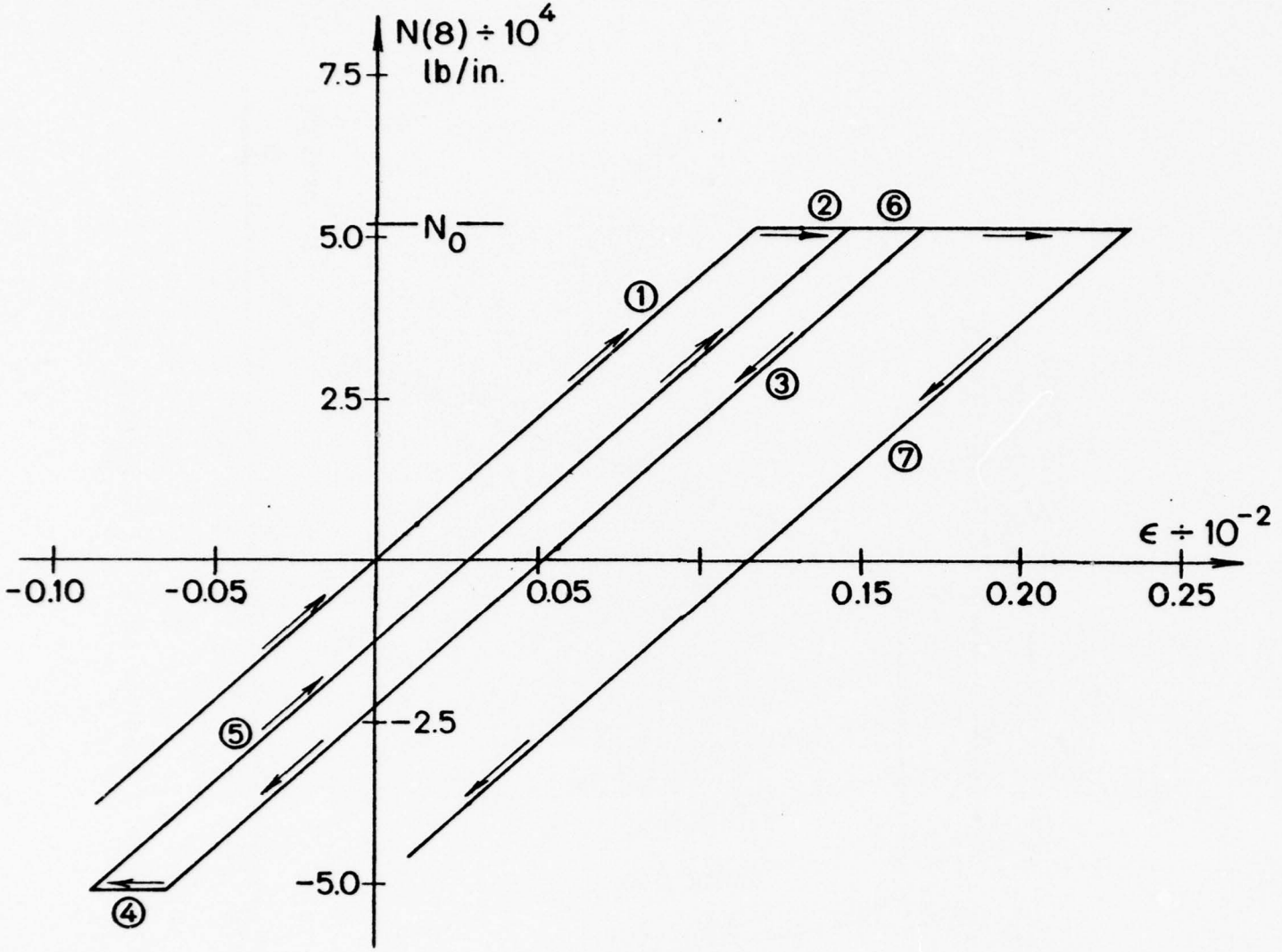

Fig. 18. Hoop stress - hoop strain diagram at grid point $\alpha = 8$

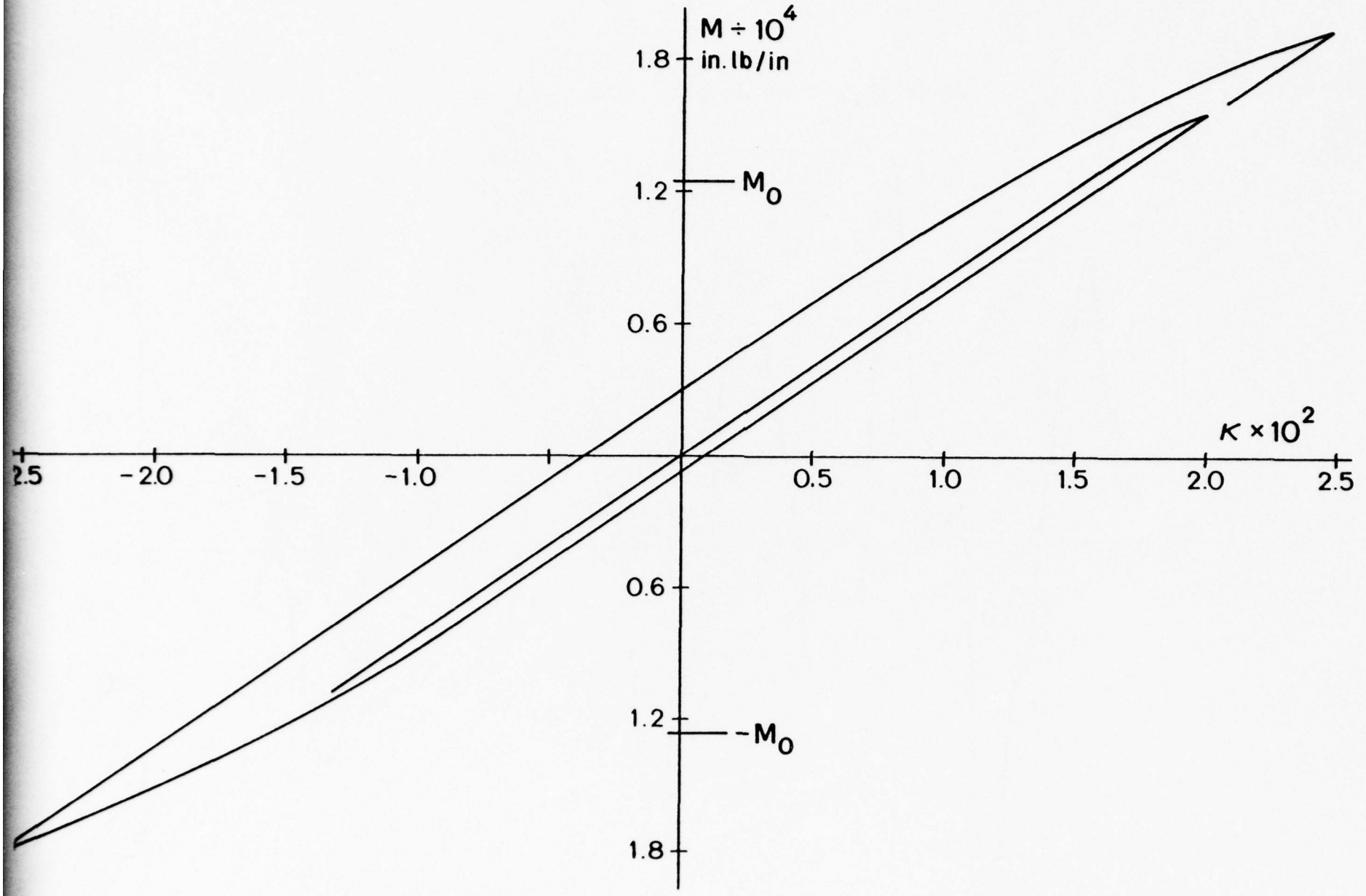

Fig. 19. Moment curvature relation at base of shell

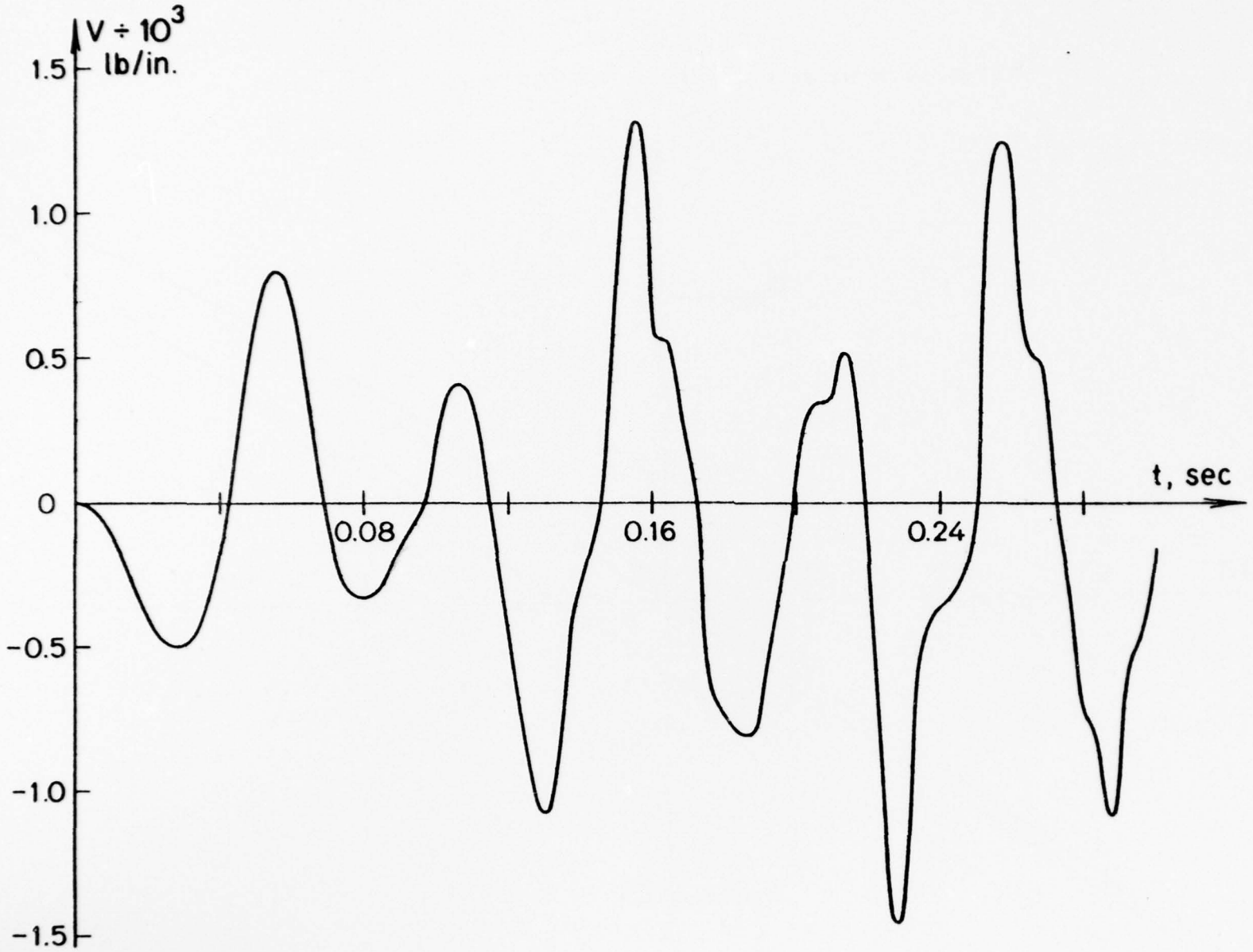

Fig. 20. Shear history at base of shell

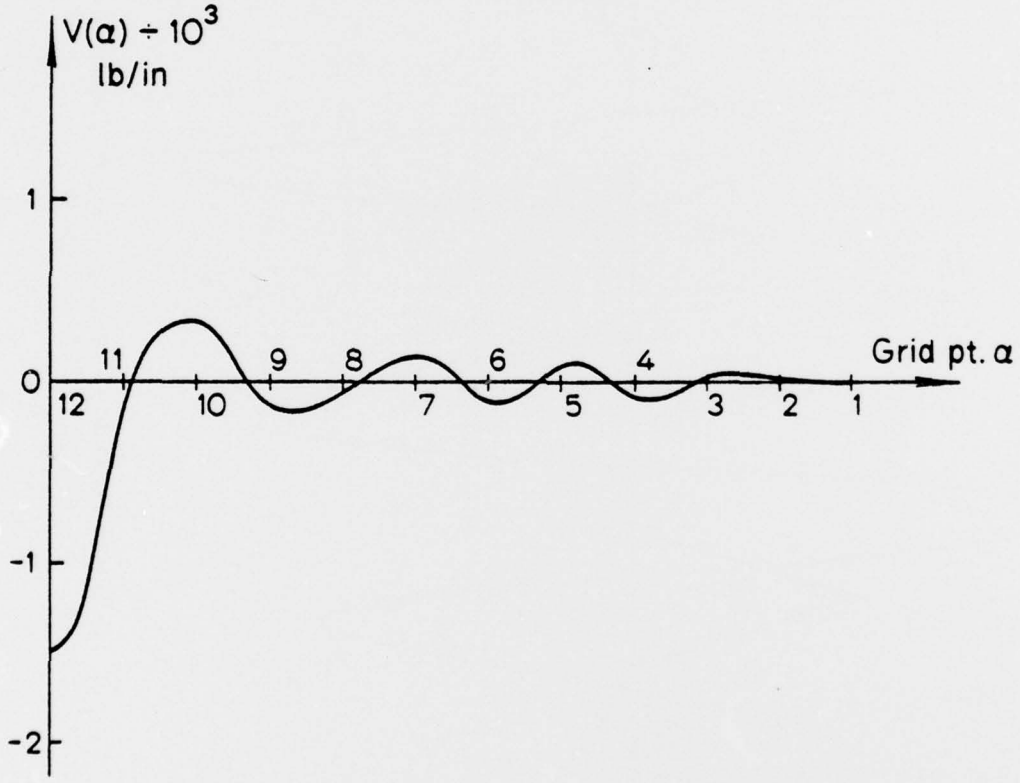

Fig. 21. Shear diagram when limit **moment first reached**

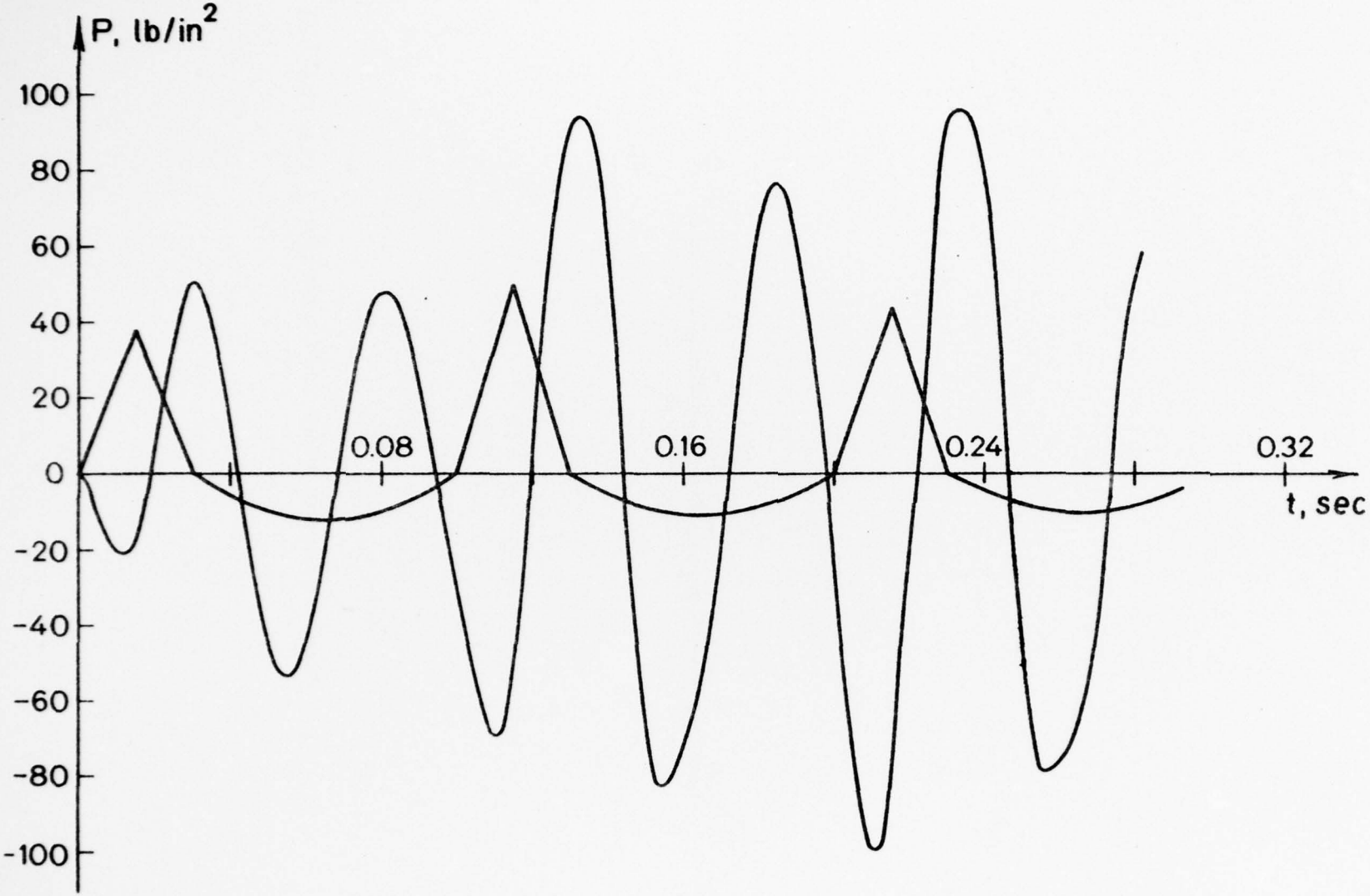

Fig. 22. History of induced fluid pressure (superimposed on incident fluid pressure) on shell wall at grid pt. $\alpha = 8$

APPENDIX III - NOTATION

The following symbols are used in this paper:

A = quantity defined by Eq. (51)

$\underline{D}$ = elastic-plastic tangent stiffness, matrix defined by Eq. (53)

E = superscript denoting elastic component.

= Young's modulus.

$\underline{E}$ = elastic modulus matrix, defined by Eq. (27)

F = loading function, defined by Eq. (37)

F_a, F_b = loading surfaces meeting at a corner. See Fig. 8.

F_1, F_2 = successive iterative approximations to F of Sec. 3.

F_o = yield function, defined by Eq. (30).

F_L = limit function, defined by Eq. (36).

G = gradient of loading function, defined by Eq. (43).

G_M = contribution to G of bending, defined by Eq. (44)

I_M = quantity defined by Eq. (32).

I_M^* = quantity defined either by Eq. (38) or (39).

I_N = quantity defined by Eq. (31).

I_{MN} = quantity defined by Eq. (33).

L = total depth of model of containment vessel. See Fig. 1.

M = subscript denoting contribution of bending moment.

= longitudinal bending moment per unit of length.

M* = hardening parameter.

M_o = yield moment in pure bending, given by Eq. (35).

M_L = limit moment in pure bending.

N = subscript denoting contribution of hoop force.

= hoop force per unit length.

N_o = axial force which causes yield in absence of bending, given by Eq. (34).

a,b = subscripts denoting two loading surfaces at a corner. See Fig. 8.

c = acoustic velocity in water.

$\underline{e}$ = total strain matrix, defined by Eq. (22).

$\underline{e}^E$, $\underline{e}^P$ = elastic and plastic components of $\underline{e}$, respectively.

h = shell wall thickness.

i = generic subscript denoting discrete time step.

k = longitudinal curvature of shell.

k_o = value of k at yield in pure bending.

k^E, k^P = elastic and plastic components of k, respectively.

ℓ = depth of elastic shell wall: See Fig. 1.

p = dynamic pressure in contained water.

p_I = incident fluid pressure on shell wall caused by cleaning of relief value.

r = radial cylindrical coordinate. See Fig. 1.

r_1, r_2, r_3 = radii of pedestal, containment vessel bottom, and shell wall, respectively. See Fig. 1.

$\underline{s}$ = stress matrix, defined by Eq. (26).

$\underline{s}_1$, $\underline{s}_2$ etc. = stress matrix iterations. See Sect. 3

t = time.

t_i = time at i th discrete interval.

u = radial component of fluid velocity.

$\underline{u}$ = (vector) fluid velocity.

v = axial component of fluid velocity.

w = (radial) displacement of shell wall, assumed positive outward.

z = axial cylindrical coordinate. See Fig. 1.

Δ = denotes temporal increment.

$\underline{\nabla}$ = (vector) gradient.

α = angular discontinuity in shell bottom. See Fig. 1.

β = quantity defined by Eq. (A1).

δ = denotes a restricted temporal rate. See Eqs. (45) and (47).

ϵ = total circumferential strain in shell well.

ϵ^E, ϵ^P = elastic and plastic components of ϵ, respectively.

λ = quantity defined by Eq. (49).

λ_a, λ_b = value of λ for two loading function at a corner.

ν = Poisson's ratio.

σ_o = uniaxial yield stress.

ρ = density of fluid.

ρ_s = density of shell wall.

SECURITY CLASSIFICATION OF THIS PAGE (When Data Entered)

REPORT DOCUMENTATION PAGE		READ INSTRUCTIONS BEFORE COMPLETING FORM
1. REPORT NUMBER 52	2. GOVT ACCESSION NO.	3. RECIPIENT'S CATALOG NUMBER
4. TITLE (and Subtitle) Dynamic Elastic-Plastic Response of a Containment Vessel to Fluid Pressure Pulses		5. TYPE OF REPORT & PERIOD COVERED Technical Report 31 Dec 1976-30 Jun 1977 6. PERFORMING ORG. REPORT NUMBER
7. AUTHOR(s) G. Nikolakopoulou and F.L. DiMaggio		8. CONTRACT OR GRANT NUMBER(s) N00014-75-C-0695 NR 064-428
9. PERFORMING ORGANIZATION NAME AND ADDRESS Columbia University, N Y. N.Y. 10027		10. PROGRAM ELEMENT, PROJECT, TASK AREA & WORK UNIT NUMBERS N00014-75-C-0695 NR 064-428
11. CONTROLLING OFFICE NAME AND ADDRESS Office of Naval Research		12. REPORT DATE February 1978 13. NUMBER OF PAGES 52
14. MONITORING AGENCY NAME & ADDRESS(if different from Controlling Office) Director, ONR Research Branch Office 495 Summer Street, Boston, Mass. 02210		15. SECURITY CLASS. (of this report) Unclassified 15a. DECLASSIFICATION/DOWNGRADING SCHEDULE

16. DISTRIBUTION STATEMENT (of this Report)

Approved for public release; distribution unlimited

17. DISTRIBUTION STATEMENT (of the abstract entered in Block 20, if different from Report)

18. SUPPLEMENTARY NOTES

19. KEY WORDS (Continue on reverse side if necessary and identify by block number)

Fluid-Structure Interaction
Plasticity
Shells

20. ABSTRACT (Continue on reverse side if necessary and identify by block number)

The dynamic analysis of the wall of a fluid-filled unstiffened nuclear containment vessel, to the fluid pressure exerted on it when the relief valve discharge piping is cleared, is extended into the plastic range using two versions of an elastic-plastic shell theory.

PART 1 - GOVERNMENT

Administrative & Liaison Activities

Chief of Naval Research
Department of the Navy
Arlingon, Virginia 22217
Attn: Code 474 (2)
471
222

Director
ONR Branch Office
495 Summer Street
Boston, Massachusetts 02210

Director
ONR Branch Office
219 S. Dearborn Street
Chicago, Illinois 60604

Director
Naval Research Laboratory
Attn: Code 2629 (ONRL)
Washington, D.C. 20390 (6)

U.S. Naval Research Laboratory
Attn: Code 2627
Washington, D.C. 20390

Commanding Officer
ONR Branch Office
207 West 24th Street
New York, N.Y. 10011

Director
ONR Branch Office
1030 E. Green Street
Pasadena, California 91101

Defense Documentation Center
Cameron Station
Alexandria, Virginia 22314 (12)

Army

Commanding Officer
U.S. Army Research Office Durham
Attn: Mr. J. J. Murray
CRD-AA-IP
Box CM, Duke Station
Durham, North Carolina 27706 2

Commanding Officer
AMXMR-ATL
Attn: Mr. R. Shea
U.S. Army Materials Res. Agency
Watertown, Massachusetts 02172

Watervliet Arsenal
MAGGS Research Center
Watervliet, New York 12189
Attn: Director of Research

Technical Library

Redstone Scientific Info. Center
Chief, Document Section
U.S. Army Missile Command
Redstone Arsenal, Alabama 35809

Army R&D Center
Fort Belvoir, Virginia 22060

Navy

Commanding Officer and Director
Naval Ship Research & Development Center
Bethesda, Maryland 20034
Attn: Code 042 (Tech. Lib. Br.)
17 (Struc. Mech. Lab.)
172
172
174
177
1800 (Appl. Math. Lab.)
5412S (Dr. W.D. Sette)
19 (Dr. M.M. Sevik)
1901 (Dr. M. Strassberg)
1945
196 (Dr. D Feit)
1962

Naval Weapons Laboratory
Dahlgren, Virginia 22448

Naval Research Laboratory
Washington, D.C. 20375
Attn: Code 8400
8410
8430
8440
6300
6390
6380

Undersea Explosion Research Div.
Naval Ship R&D Center
Norfolk Naval Shipyard
Portsmouth, Virginia 23709
Attn: Dr. E. Palmer
Code 780

Naval Ship Research & Development Center
Annapolis Division
Annapolis, Maryland 21402
Attn: Code 2740 - Dr. Y.F. Wang
28 - Mr. R.J. Wolfe
281 - Mr. R.B. Niederberger
2814 - Dr. H. Vanderveldt

Technical Library
Naval Underwater Weapons Center
Pasadena Annex
3202 E. Foothill Blvd.
Pasadena, California 91107

U.S. Naval Weapons Center
China Lake, California 93557
Attn: Code 4062 - Mr. W. Werback
4520 - Mr. Ken Bischel

Commanding Officer
U.S. Naval Civil Engr. Lab.
Code L31
Port Hueneme, California 93041

Technical Director
U.S. Naval Ordnance Laboratory
White Oak
Silver Spring, Maryland 20910

Technical Director
Naval Undersea R&D Center
San Diego, California 92132

Supervisor of Shipbuilding
U.S. Navy
Newport News, Virginia 23607

Technical Director
Mare Island Naval Shipyard
Vallejo, California 94592

U.S. Navy Underwater Sound Ref. Lab.
Office of Naval Research
P.O. Box 8337
Orlando, Florida 32806

Chief of Naval Operations
Dept. of the Navy
Washington, D.C. 20350
Attn: Code Op07T

Strategic Systems Project Office
Department of the Navy
Washington, D.C. 20390
Attn: NSP-001 Chief Scientist

Deep Submergence Systems
Naval Ship Systems Command
Code 39522
Department of the Navy
Washington, D.C. 20360

Engineering Dept.
U.S. Naval Academy
Annapolis, Maryland 21402

Naval Air Systems Command
Dept. of the Navy
Washington, D.C. 20360
Attn: NAVAIR 5302 Aero & Structures
5308 Structures
52031F Materials
604 Tech. Library
320B Structures

Director, Aero Mechanics
Naval Air Development Center
Johnsville
Warminster, Pennsylvania 18974

Technical Director
U.S. Naval Undersea R&D Center
San Diego, California 92132

Engineering Department
U.S. Naval Academy
Annapolis, Maryland 21402

Naval Facilities Engineering Command
Dept. of the Navy
Washington, D.C. 20360
Attn: NAVFAC 03 Research & Development
04 " "
14114 Tech. Library

Naval Sea Systems Command
Dept. of the Navy
Washington, D.C. 20360
Attn: NAVSHIP 03 Res. & Technology
031 Ch. Scientist for R&D
03412 Hydromechanics
037 Ship Silencing Div.
035 Weapons Dynamics

Naval Ship Engineering Center
Prince George's Plaza
Hyattsville, Maryland 20782
Attn: NAVSEC 6100 Ship Sys Engr & Des Dep
6102C Computer-Aided Ship Des
6105G
6110 Ship Concept Design
6120 Hull Div.
6120D Hull Div.
6128 Surface Ship Struct.
6129 Submarine Struct.

Air Force

Commander WADD
Wright-Patterson Air Force Base
Dayton, Ohio 45433
Attn: Code WWRMDD
AFFDL (FDDS)
Structures Division
AFLC (MCEEA)

Chief, Applied Mechanics Group
U.S. Air Force Inst. of Tech.
Wright-Patterson Air Force Base
Dayton, Ohio 45433

Chief, Civil Engineering Branch
WLRC, Research Division
Air Force Weapons Laboratory
Kirtland AFB, New Mexico 87117

Air Force Office of Scientific Research
1400 Wilson Blvd.
Arlington, Virginia 22209
Attn: Mechanics Div.

NASA

Structures Research Division
National Aeronautics & Space Admin.
Langley Research Center
Langley Station
Hampton, Virginia 23365

National Aeronautic & Space Admin.
Associate Administrator for Advanced
Research & Technology
Washington, D.C. 02546

Scientific & Tech. Info. Facility
NASA Representative (S-AK/DL)
P.O. Box 5700
Bethesda, Maryland 20014

Other Government Activities

Commandant
Chief, Testing & Development Div.
U.S. Coast Guard
1300 E. Street, N.W.
Washington, D.C. 20226

Technical Director
Marine Corps Dev. & Educ. Command
Quantico, Virginia 22134

Director
National Bureau of Standards
Washington, D.C. 20234
Attn: Mr. B.L. Wilson, EM 219

Dr. M. Gaus
National Science Foundation
Engineering Division
Washington, D.C. 20550

Science & Tech. Division
Library of Congress
Washington, D.C. 20540

Director
Defense Nuclear Agency
Washington, D.C. 20305
Attn: SPSS

Commander Field Command
Defense Nuclear Agency
Sandia Base
Albuquerque, New Mexico 87115

Director Defense Research & Engrg
Technical Library
Room 3C-128
The Pentagon
Washington, D.C. 20301

Chief, Airframe & Equipment Branch
FS-120
Office of Flight Standards
Federal Avaiation Agency
Washington, D.C. 20553

Chief, Research and Development
Maritime Administration
Washington, D.C. 20235

Deputy Chief, Office of Ship Constr.
Maritime Administration
Washington, D.C. 20235
Attn: Mr. U.L. Russo

Atomic Energy Commission
Div. of Reactor Devel. & Tech.
Germantown, Maryland 20767

Ship Hull Research Committee
National Research Council
National Academy of Sciences
2101 Constitution Avenue
Washington, D.C. 20418
Attn: Mr. A.R. Lytle

PART 2 - CONTRACTORS AND OTHER TECHNICAL COLLABORATORS

Universities

Dr. J. Tinsley Oden
University of Texas at Austin
345 Eng. Science Bldg.
Austin, Texas 78712

Prof. Julius Miklowitz
California Institute of Technology
Div. of Engineering & Applied Sciences
Pasadena, California 91109

Dr. Harold Liebowitz, Dean
School of Engr. & Applied Science
George Washington University
725 - 23rd St., N.W.
Washington, D.C. 20006

Prof. Eli Sternberg
California Institute of Technology
Div. of Engr. & Applied Sciences
Pasadena, California 91109

Prof. Paul M. Naghdi
University of California
Div. of Applied Mechanics
Etcheverry Hall
Berkeley, California 94720

Professor P. S. Symonds
Brown University
Division of Engineering
Providence, R.I. 02912

Prof. A. J. Durelli
The Catholic University of America
Civil/Mechanical Engineering
Washington, D.C. 20017

Prof. R.B. Testa
Columbia University
Dept. of Civil Engineering
S.W. Mudd Bldg.
New York, N.Y. 10027

Prof. H. H. Bleich
Columbia University
Dept. of Civil Engineering
Amsterdam & 120th St.
New York, N.Y. 10027

Prof. F.L. DiMaggio
Columbia University
Dept. of Civil Engineering
616 Mudd Building
New York, N.Y. 10027

Prof. A.M. Freudenthal
George Washington University
School of Engineering & Applied Science
Washington, D.C. 20006

D. C. Evans
University of Utah
Computer Science Division
Salt Lake City, Wash 84112

Prof. Norman Jones
Massachusetts Inst. of Technology
Dept. of Naval Architecture & Marine Engrng
Cambridge, Massachusetts 02139

Professor Albert I. King
Biomechanics Research Center
Wayne State University
Detroit, Michigan 48202

Dr. V. R. Hodgson
Wayne State University
School of Medicine
Detroit, Michigan 48202

Dean B. A. Boley
Northwestern University
Technological Institute
2145 Sheridan Road
Evanston, Illinois 60201

Prof. P.G. Hodge, Jr.
University of Minnesota
Dept. of Aerospace Engng & Mechanics
Minneapolis, Minnesota 55455

Dr. D.C. Drucker
University of Illinois
Dean of Engineering
Urbana, Illinois 61801

Prof. N.M. Newmark
University of Illinois
Dept. of Civil Engineering
Urbana, Illinois 61801

Prof. E. Reissner
University of California, San Diego
Dept. of Applied Mechanics
La Jolla, California 92037

Prof. William A. Nash
University of Massachusetts
Dept. of Mechanics & Aerospace Engng.
Amherst, Massachusetts 01002

Library (Code 0384)
U.S. Naval Postgraduate School
Monterey, California 93940

Prof. Arnold Allentuch
Newark College of Engineering
Dept. of Mechanical Engineering
323 High Street
Newark, New Jersey 07102

Dr. George Herrmann
Stanford University
Dept. of Applied Mechanics
Stanford, California 94305

Prof. J. D. Achenbach
Northwestern University
Dept. of Civil Engineering
Evanston, Illinois 60201

Director, Applied Research Lab.
Pennsylvania State University
P. O. Box 30
State College, Pennsylvania 16801

Prof. Eugen J. Skudrzyk
Pennsylvania State University
Applied Research Laboratory
Dept. of Physics - P.O. Box 30
State College, Pennsylvania 16801

Prof. J. Kempner
Polytechnic Institute of Brooklyn
Dept. of Aero.Engrg.& Applied Mech
333 Jay Street
Brooklyn, N.Y. 11201

Prof. J. Klosner
Polytechnic Institute of Brooklyn
Dept. of Aerospace & Appl. Mech.
333 Jay Street
Brooklyn, N.Y. 11201

Prof. R.A. Schapery
Texas A&M University
Dept. of Civil Engineering
College Station, Texas 77840

Prof. W.D. Pilkey
University of Virginia
Dept. of Aerospace Engineering
Charlottesville, Virginia 22903

Dr. H.G. Schaeffer
University of Maryland
Aerospace Engineering Dept.
College Park, Maryland 20742

Prof. K.D. Willmert
Clarkson College of Technology
Dept. of Mechanical Engineering
Potsdam, N.Y. 13676

Dr. J.A. Stricklin
Texas A&M University
Aerospace Engineering Dept.
College Station, Texas 77843

Dr. L.A. Schmit
University of California, LA
School of Engineering & Applied Science
Los Angeles, California 90024

Dr. H.A. Kamel
The University of Arizona
Aerospace & Mech. Engineering Dept.
Tucson, Arizona 85721

Dr. B.S. Berger
University of Maryland
Dept. of Mechanical Engineering
College Park, Maryland 20742

Prof. G. R. Irwin
Dept. of Mechanical Engrg.
University of Maryland
College Park, Maryland 20742

Dr. S.J. Fenves
Carnegie-Mellon University
Dept. of Civil Engineering
Schenley Park
Pittsburgh, Pennsylvania 15213

Dr. Ronald L. Huston
Dept. of Engineering Analysis
Mail Box 112
University of Cincinnati
Cincinnati, Ohio 45221

Prof. George Sih
Dept. of Mechanics
Lehigh University
Bethlehem, Pennsylvania 18015

Prof. A.S. Kobayashi
University of Washington
Dept. of Mechanical Engineering
Seattle, Washington 98105

Librarian
Webb Institute of Naval Architecture
Crescent Beach Road, Glen Cove
Long Island, New York 11542

Prof. Daniel Frederick
Virginia Polytechnic Institute
Dept. of Engineering Mechanics
Blacksburg, Virginia 24061

Prof. A.C. Eringen
Dept. of Aerospace & Mech. Sciences
Princeton University
Princeton, New Jersey 08540

Dr. S.L. Koh
School of Aero., Astro.& Engr. Sc.
Purdue University
Lafayette, Indiana 47907

Prof. E.H. Lee
Div. of Engrg. Mechanics
Stanford University
Stanford, California 94305

Prof. R.D. Mindlin
Dept. of Civil Engrg.
Columbia University
S.W. Mudd Building
New York, N.Y. 10027

Prof. S.B. Dong
University of California
Dept. of Mechanics
Los Angeles, California 90024

Prof. Burt Paul
University of Pennsylvania
Towne School of Civil & Mech. Engrg.
Rm. 113 - Towne Building
220 S. 33rd Street
Philadelphia, Pennsylvania 19104

Prof. H.W. Liu
Dept. of Chemical Engr. & Metal.
Syracuse University
Syracuse, N.Y. 13210

Prof. S. Bodner
Technion R&D Foundation
Haifa, Israel

Prof. R.J.H. Bollard
Chairman, Aeronautical Engr. Dept.
207 Guggenheim Hall
University of Washington
Seattle, Washington 98105

Prof. G.S. Heller
Division of Engineering
Brown University
Providence, Rhode Island 02912

Prof. Werner Goldsmith
Dept. of Mechanical Engineering
Div. of Applied Mechanics
University of California
Berkeley, California 94720

Prof. J.R.Rice
Division of Engineering
Brown University
Providence, Rhode Island 02912

Prof. R.S. Rivlin
Center for the Application of Mathematics
Lehigh University
Bethlehem, Pennsylvania 18015

Library (Code 0384)
U.S. Naval Postgraduate School
Monterey, California 93940

Dr. Francis Cozzarelli
Div. of Interdisciplinary
Studies & Research
School of Engineering
State University of New York
Buffalo, N.Y. 14214

Industry and Research Institutes

Library Services Department
Report Section Bldg. 14-14
Argonne National Laboratory
9700 S. Cass Avenue
Argonne, Illinois 60440

Dr. M. C. Junger
Cambridge Acoustical Associates
129 Mount Auburn St.
Cambridge, Massachusetts 02138

Dr. L.H. Chen
General Dynamics Corporation
Electric Boat Division
Groton, Connecticut 06340

Dr. J.E. Greenspon
J.G. Engineering Research Associates
3831 Menlo Drive
Baltimore, Maryland 21215

Dr. S. Batdorf
The Aerospace Corp.
P.O. Box 92957
Los Angeles, California 90009

Dr. K.C. Park
Lockheed Palo Alto Research Laboratory
Dept. 5233, Bldg. 205
3251 Hanover Street
Palo Alto, CA 94304

Library
Newport News Shipbuilding &
Dry Dock Company
Newport News, Virginia 23607

Dr. W.F. Bozich
McDonnell Douglas Corporation
5301 Bolsa Ave.
Huntington Beach, CA 92647

Dr. H.N. Abramson
Southwest Research Institute
Technical Vice President
Mechanical Sciences
P.O. Drawer 28510
San Antonio, Texas 78284

Dr. R.C. DeHart
Southwest Research Institute
Dept. of Structural Research
P.O. Drawer 28510
San Antonio, Texas 78284

Dr. M.L. Baron
Weidlinger Associates,
Consulting Engineers
110 East 59th Street
New York, N.Y. 10022

Dr. W.A. von Riesemann
Sandia Laboratories
Sandia Base
Albuquerque, Ney Mexico 87115

Dr. T.L. Geers
Lockheed Missiles & Space Co.
Palo Alto Research Laboratory
3251 Hanover Street
Palo Alto, California 94304

Dr. J.L. Tocher
Boeing Computer Services, Inc.
P.O. Box 24346
Seattle, Washington 98124

Mr. Willian Caywood
Code BBE, Applied Physics Laboratory
8621 Georgia Avenue
Silver Spring, Maryland 20034

Mr. P.C. Durup
Lockheed-California Company
Aeromechanics Dept., 74-43
Burbank, California 91503

Assistant Chief for Technology
Office of Naval Research,
Code 200
Arlongton, Virginia 22217